Swansea University
Prifysgol Abertawe

Cronfa
Setting Research Free

Cronfa - Swansea University Open Access Repository

_____

This is an author produced version of a paper published in :
International Journal of Hydrogen Energy

_____

Cronfa URL for this paper:
http://cronfa.swan.ac.uk/Record/cronfa18611

_____

_____

Influence of grain boundary misorientation on hydrogen embrittlement in bi-crystal nickel.

*S. Jothi, T. N. Croft, S. G. R. Brown

College of Engineering, Swansea University, Singleton Park, Swansea SA2 8PP, UK
*S.Jothi@swansea.ac.uk

ABSTRACT

Computational techniques and tools have been developed to understand hydrogen embrittlement and hydrogen induced intergranular cracking based on grain boundary (GB) engineering with the help of computational materials engineering. This study can help to optimize GB misorientation configurations by identifying the cases that would improve the material properties increasing resistance to hydrogen embrittlement. In order to understand and optimize, it is important to understand the influence of misorientation angle on the atomic clustered hydrogen distribution under the impact of dilatational stress distributions. In this study, a number of bi-crystal models with tilt grain boundary (TGB) misorientation angles (θ) ranging between $0° \leq \theta \leq 90°$ were developed, with rotation performed about the [001] axis, using numerical microstructural finite element analysis. Subsequently, local stress and strain concentrations generated along the TGB (due to the difference in individual neighbouring crystals elastic anisotropy response as functions of misorientation angles) were evaluated when bi-crystals were subjected to overall uniform applied traction. Finally, the hydrogen distribution and segregations as a function of misorientation angles were studied. In real nickel, as opposed to the numerical model, geometrically necessary dislocations are generated due to GB misorientation. The generated dislocation motion along TGBs in response to dilatational mismatch varies depending on the misorientation angles. These generated dislocation motions affect the stress, strain and hydrogen distribution. Hydrogen segregates along these dislocations acting as traps and since the dislocation distribution varies depending on misorientation angles the hydrogen traps are also influenced by misorientation angles. From the results of numerical modelling it has been observed that the local stress, strain and hydrogen distributions are inhomogeneous, affected by the misorientation angles, orientations of neighbouring crystal and boundary conditions. In real material, as opposed to the numerical model, the clustered atomic hydrogens are segregated in traps near to the TGB due to the influence of dislocations developed under the effects of applied mechanical stress. The numerical model predicts maximum hydrogen concentrations are accumulated on the TGB with misorientation angles ranging between $15°<\theta<45°$. This investigation reinforces the importance of GB engineering for designing and optimizing these materials to decrease hydrogen segregation arising from TGB misorientation angles.

Keywords: Hydrogen Embrittlement; Misorientation; Grain boundary engineering, Tilt grain boundary; Stress induced hydrogen cracking; Finite element analysis; Bi-crystal nickel;

1. Introduction

Crystallographic interfaces and micro-textures such as GB misorientation are characterized by specific arrangements of their atoms. They play a prominent role in aerospace components which are typically made of high strength, high toughness, and corrosion resistant as well as high temperature metallic materials such as nickel, titanium and

nickel-based super alloys. Nickel and nickel-based super alloys are made up of complex microstructures and have been used in aerospace applications for many years. Several catastrophic failures have occurred in nickel and nickel-based super alloys in aerospace components due to environmental cracking, hydrogen stress cracking and hydrogen embrittlement [1-4, 53]. Hydrogen embrittlement is a costly problem in which structural degradation of the susceptible material leads to catastrophic failure. Atomic impurities in structural materials may occur any time during its life time, during fabrication in a manufacturing process or during operational use under service environmental conditions. It is not only a problem in the aerospace industries but also in many other sectors such as automotive, civil and construction, semiconductor, offshore, ship, oil and gas, nuclear power and renewable energy including wind energy, fuel cells and hydrogen energy. The susceptibility of structural materials to hydrogen embrittlement depends on many factors including hydrogen atom-microstructural interactions [1, 3, 11-12], microstructural intergranular engineering [6-8] and texture morphological behaviour [8-10]. By understanding and controlling some of these factors the susceptibility of materials can be reduced [12-16]. Even though there is a considerable amount of information available regarding the relationship between crystallographic micro-textures of materials such as TGB misorientation angles and hydrogen induced stress cracking [7, 17-18], there has not been enough research done implementing this information into computational tools in order to understand material design and material design optimization based on GB engineering using finite element analysis (FEA). It is important to understand both the GB engineering and the relationship between misorientation angle and chemical and mechanical material degradation and properties at the design stage to develop new materials and to optimize existing materials to improve efficiency and increase the resistance of materials to hydrogen induced intergranular cracking, ideally implementing this approach into industrially applicable simulations.

The presence of GBs, interphase boundaries and the segregation of impurities are affected by GB misorientation significantly affects chemical, and mechanical properties as well as fracture processes such as crack nucleation and crack propagation in textured polycrystalline metallic materials [5-10]. It is already known that high densities of GBs (i.e. grain size), the type of GBs and GB misorientations with specific angles are important and could be optimized to increase properties such as strength, ductility and fracture toughness of textured polycrystalline metallic materials. On the other hand, GBs and GB misorientation can also be

potential sites for segregation of impurities, cracks, fractures and their behaviour is responsible for GB embrittlement depending on the characteristics of the GBs misorientations within them [9-20]. It has been recently found that low angle grain boundaries and low Σ coincidence boundaries or coincidence site lattices (CSL) are immune to intergranular fractures that lead to intergranular cracking and intergranular embrittlement [9-10]. On the other hand high angle boundaries are preferential sites for fractures leading to crack nucleation and propagation [9-10, 12-13]. Watanabe introduced the concept of 'grain boundary design and control' suggesting that GB misorientation and grain boundary character distribution (GBCD) are key microstructural parameters controlling the fracture toughness of polycrystalline metallic material [6-12]. Palumbo developed this concept as grain boundary engineering (GBE) and improved intergranular susceptibility by implementing GBE in nickel-based super alloys [21, 11-16]. The GB misorientation and the distributions of GB misorientation angles are important parameters controlling the propensity of segregation of impurities and stress induced hydrogen fractures that can lead to catastrophic GB embrittlement failure of textured polycrystalline metallic materials. It is well known from the literature that texture and GB misorientation play important role in the impurities induced cracking [6-20]. Therefore, it would be of interest to implement GB misorientation in finite element modelling and develop a procedure to quantify the effect of GB misorientation and crystallographic texture on the stress induced mass diffusion of impurities in polycrystalline textured nickel developed for aerospace applications.

Most existing studies of the effect of environmental impurities (i.e. sulphur, hydrogen, oxygen, boron etc.) on embrittlement and cracking mechanisms in polycrystalline structural materials are based on global, macro mechanical properties. However microstructural inhomogeneity and micro-texture can result in micro-cracks and dislocation formation which may lead to macroscopic environmental failures of polycrystalline materials [1-4]. Since a polycrystalline material is an aggregate of crystal grains of various sizes and shapes, its macroscopic properties are affected by the properties of individual grains. Each individual crystal in polycrystalline nickel may exhibit elastic anisotropy due to its crystal symmetric characteristics. The elastic deformation of single crystals may exhibit anisotropy depending on the orientation of the crystal. The presence of microstructural inhomogeneity, morphological and crystallographic textures will certainly affect the correlation between experimental observation and prediction based on an assumed homogeneous deformation [22-26]. So with a better understanding of microstructurally local behaviour of high

performance polycrystalline materials, the embrittlement problem may be reduced or perhaps solved by expanding the concept of microstructural local behaviour of polycrystalline engineering structural materials into design and analysis.

The local microstructural multi-physics stress induced hydrogen behaviours of the materials are strongly affected by the GB misorientation angles. The macroscopic environmental embrittlement cracking behaviour of materials is associated with local dislocation, stresses generated at the interface between crystals due to the GB misorientation angles and the accumulation, and segregation of hydrogen to these dislocations. Segregation of hydrogen has been experimentally observed at GBs in bi-crystal, and polycrystalline nickel and an increase in the amount of segregated hydrogen increases the possibility of intergranular hydrogen embrittlement where the fracture mode is observed along the intergranular region [3, 27-28]. It has also been observed that GB misorientation angle affects the GB diffusion of hydrogen in a material [29-30]. Thus, it is important to understand the relationship between GB misorientation angle and hydrogen segregation in nickel. The GB misorientation angle that allows the highest segregation of hydrogen along the GBs plays a key role in determining the structural integrity of nickel when considering intergranular hydrogen embrittlement.

The geometric distribution of grains shapes, size, grain boundary length and statistical distributions of GB misorientation angles of the metallic materials can be acquired experimentally using the electron back scattering diffraction (EBSD) technique and X-ray diffraction [31-33]. The Voronoi tessellation technique is a well-established approximation technique used to model the actual microstructure of bi-crystal polycrystalline materials and GB misorientation. The angle of rotation between different crystals can be assigned directly onto a meso-scale microstructural framework consisting of a Voronoi tessellation [33-34]. The advantage of FEA simulation of bi-crystal and polycrystalline materials is that GB misorientation angles, crystallographic morphology and textures such as grain size and shape of the grains can be defined as needed. The meso-scale microstructural polycrystalline model can be embedded into a macro scale continuum model [35-38]. Thus it may be possible to computationally study the relation between GB misorientation angles and stress/strain distribution and hydrogen embrittlement using FEA. If the FEA is performed before processing specimens for a real bi-crystal and polycrystalline, characteristics of localized stress, strain, hydrogen distribution in mesostructure can be predicted.

In the mechanical stress analysis of bi-crystal and polycrystalline aggregates, the local microstructural elastic deformation behaviour of individual FCC single crystal structures will generally be anisotropic and exhibits orthotropic behaviour in nature [39-42]. Previous research by den Toonder et al [40] concluded that using the average isotropic elastic properties is incorrect for cubic bi-crystal and polycrystalline aggregate microstructures. FCC crystals are mechanically anisotropic due to the orientation dependence of the activation of the crystallographic deformation mechanism, and with other mechanical phenomena such as strength, shape change and crystallographic texture (orientation distribution) etc. [41,43].

In the present study, the main interest is to investigate the influence of TGB misorientation angles on stress, strain and hydrogen distribution and segregation in nickel. In order to understand low resistance as well as high resistance to environmental hydrogen fractures and hydrogen embrittlement in nickel at design stage, it is important to understand the influence of misorientation angle on hydrogen distribution.

A finite element multi-physics meso-scale bi-crystal model has been developed for nickel that includes the effect of TGB misorientation angles. Continuum level stress induced solid state atomic hydrogen diffusion analyses of bi-crystal nickel have been performed for various misorientation angles (θ) ranging between $0° \leq \theta \leq 90°$ with rotation performed about the [001] axis, subjected to mechanical tension along the [010] direction. In these analyses the coupling of TGB misorientation angles, hydrostatic stress field and solid state atomic hydrogen diffusion was considered. The effect of various TGB misorientation angles on the mechanical stress distribution using stress analysis was examined. Transient hydrogen diffusion analysis coupled with the mechanical stress analysis of the bi-crystal nickel was performed for the chosen misorientation angles.

2. Computational methods:

2.1   A mathematical description of stress induced hydrogen diffusion:

The hydrogen flux vector J consists of a combination of hydrogen generated by the hydrogen concentration gradient J_c and by the hydrostatic stress gradient J_h in the heterogeneous microstructural material. The hydrogen flux vector generated by the hydrogen concentration gradient is based on *Fick's first law of diffusion* by using the *thermodynamic formulation* based on the *Gibbs free enthalpy*. The hydrogen flux vector generated by the hydrostatic stress gradient is based on a *modified Fick's first law* by taking into account the stress field where the concentration of hydrogen is C, ideal gas constant R equal to 8.314

Nm/mol K, partial molar volume of hydrogen V_h (2000 mm^3/mol) [54], gradient operator∇, Laplace operator Δ and X represents three dimensions (3D) x,y,z.

$$J(X,t) = J_c(X,t) + J_h(X,t) \tag{1}$$

$$J_c(X,t) = -D\nabla C = -D\left(\frac{\partial C(x,t)}{\partial x} + \frac{\partial C(y,t)}{\partial y} + \frac{\partial C(z,t)}{\partial z}\right)) \tag{2}$$

$$J_c(X,t) = -D\frac{\partial C(X,t)}{\partial X} \tag{3}$$

$$J_h(X,t) = \frac{DV_h}{RT}C\nabla\sigma_h \tag{4}$$

$$J_h(X,t) = \frac{DV_h}{RT}C\frac{\partial\sigma_h}{\partial X} \tag{5}$$

$$\therefore J(X,t) = -D\frac{\partial C(X,t)}{\partial X} + \frac{DV_h}{RT}C\frac{\partial\sigma_h}{\partial X} \tag{6}$$

Hydrostatic stresses σ_h is defined as

$$\sigma_h = \frac{1}{3}(\sigma_{xx} + \sigma_{yy} + \sigma_{zz}) \tag{7}$$

Based on the *law of matter conservation*, the amount of hydrogen is expressed by the continuity equation based on a transient (time dependent) diffusion process without trapping as described by *Fick's second law*

$$\frac{\partial C}{\partial t} = -divJ \tag{8}$$

$$\frac{\partial C}{\partial t} = D\nabla^2 C - \frac{DV_h}{RT}(C\nabla^2\sigma_h + \nabla C\nabla\sigma_h) \tag{9}$$

$$\frac{\partial C}{\partial t} = D\frac{\partial^2 C(X,t)}{\partial X^2} - \frac{DV_h}{RT}C\frac{\partial^2\sigma_h}{\partial X^2} - \frac{DV_h}{RT}\frac{\partial\sigma_h}{\partial X}\frac{\partial C}{\partial X} \tag{10}$$

$$\therefore \frac{\partial C}{\partial t} = D\Delta C - \frac{DV_h}{RT}C\Delta\sigma_h - \frac{DV_h}{RT}\nabla C\nabla\sigma_h \tag{11}$$

The commercial software ABAQUS implements the governing equation for stress driven diffusion as shown in equation (12).

$$\therefore \frac{\partial C}{\partial t} = sD\Delta\phi - \frac{DV_h}{R(T-T_0)}s\phi\Delta\sigma_h - \frac{DV_h}{R(T-T_0)}s\nabla\phi\nabla\sigma_h \tag{12}$$

Where s is solubility, $T_0 = 0K$ and C/s is the normalized hydrogen concentration which is dependent on the hydrostatic stresses as expressed in the equation below.

$$\phi = \phi_0 exp\left(\frac{-V_h\sigma_h}{R(T-T_0)}\right) \tag{13}$$

Where the unstressed state of the normalized concentration under the condition of hydrogen-metal equilibrium is ϕ_0.

2.2   A numerical finite element approach for stress induced hydrogen diffusion:

The standard Galerkin process of the element shape functions $N_j(r)$ were used to approximate the distribution of stresses as shown in the equation (14).

$$\sigma_h(r) = \sum \sigma_{hj} N_j(r) \tag{14}$$

Where approximate distributions of stresses are $\sigma_h(r)$ and element shape functions $N_j(r)$ serve as trial and weight residual functions, $j=1,2,3,\ldots,n$ are the number of nodes of the finite element mesh. In order to apply equation (13) in finite element analysis of stress assisted diffusion, equation (12) is converted to its discrete form given by equation (15).

$$[M_{ij}]\left\{\frac{dC_j}{dt}\right\} + \left([K_{ij}^l] + [K_{ij}^l] + [K_{ij}^l]\right)\{C_j\} = \{F_i\} \tag{15}$$

Where $i=1,2,3,\ldots,n$, $\{\ldots\}$ represents the component vector column, $[\ldots]$ represents components element matrices, $[M_{ij}]$ represents the concentration capacity matrix given by equation (16), $[K_{ij}^l]$ represents the diffusion matrix given by equations (17), (18) and (19), where $\ell = 1,2,3$ and $[F_i]$ represents the diffusion flux vector columns given by equation (20).

$$[M_{ij}] = \int_V N_i N_j \, dV = \int_V [A]^T [A] \, dV \tag{16}$$

$$[K_{ij}^1] = D \int \nabla N_i \nabla N_j dV = D \int [B]^T [B] dV \tag{17}$$

$$[K_{ij}^2] = -\frac{D V_h}{R(T - T_0)} \int [A]^T [B]\{\sigma_h\}[B] dV \tag{18}$$

$$[K_{ij}^3] = -\frac{D V_h}{R(T - T_0)} \int [B]^T [B]\{\sigma_h\}[A] dV \tag{19}$$

$$[F_i] = -J_s \int_S N_i dS = \int_S [A]^T \emptyset dS \tag{20}$$

Where $\emptyset = D\nabla C - \frac{D V_h}{R(T - T_0)}$,

The interpolation matrices are [A] and [B] are given in equations (21) to (24).

$$C_j = [A]\{C_j\} \tag{21}$$

$$\frac{dC_j}{dt} = [A]\{\frac{dC_j}{dt}\} \tag{22}$$

$$\nabla\sigma_h = [B]\{\sigma_h\} \tag{23}$$

$$\nabla C = [B]\{C_j\} \tag{24}$$

The time integration in transient hydrogen concentration $\{\frac{dC_j}{dt}\}$ utilizes the modified Crank-Nicholson method is given in equation (25).

$$\left\{\frac{dC_j}{dt}\right\} = \frac{1}{\Delta t}\left(\{C_j\}_{t+\Delta t} - \{C_j\}_t\right) \tag{25}$$

The final equation is given by equation (26).

$$\left(\frac{1}{\Delta t}[M_{ij}] + [K_{ij}^1]\right)\{C_j\}_{t+\Delta t} = \left(\frac{1}{\Delta t}[M_{ij}] - [K_{ij}^2] - [K_{ij}^3]\right)\{C_j\}_t + \{F_i\} \tag{26}$$

2.3   Bi-crystal model:

The macroscopic elastic behaviour of bi-crystal and polycrystalline FCC nickel aggregates is affected by the microscopic properties such as morphological texture, random crystallographic orientations of individual grains [25, 44-47]. So the current model considers the anisotropic effect in the microstructural polycrystalline model by assigning random crystallographic orientations in each crystal using the FCC nickel single crystal anisotropic elastic constants as shown in equation (30) [41]. The short review of elastic theory below shows the relationship between the macroscopic isotropic behaviour of bi-crystals, polycrystalline aggregates and local microscopic anisotropic behaviour of single crystals.

$$\sigma_{ij} = C_{ijkl} : \varepsilon_{kl} \tag{27}$$

$$\varepsilon_{kl} = \frac{1}{2}(\nabla u + (\nabla u)^T) \tag{28}$$

Where σ is the Cauchy stress tensor, C is the fourth order anisotropic elastic tensor, ε is the strain tensor and u is displacement, ij is direction and kl is plane, i, j, k and l can represent x, y or z axes.

$$\begin{bmatrix} \sigma_{11} \\ \sigma_{22} \\ \sigma_{33} \\ \sigma_{23} \\ \sigma_{31} \\ \sigma_{12} \end{bmatrix} = \begin{bmatrix} C_{1111} & C_{1122} & C_{1122} & 0 & 0 & 0 \\ C_{1122} & C_{1111} & C_{1122} & 0 & 0 & 0 \\ C_{1122} & C_{1122} & C_{1111} & 0 & 0 & 0 \\ 0 & 0 & 0 & C_{2323} & 0 & 0 \\ 0 & 0 & 0 & 0 & C_{2323} & 0 \\ 0 & 0 & 0 & 0 & 0 & C_{2323} \end{bmatrix} \begin{bmatrix} \varepsilon_{11} \\ \varepsilon_{22} \\ \varepsilon_{33} \\ \varepsilon_{23} \\ \varepsilon_{31} \\ \varepsilon_{12} \end{bmatrix} \tag{29}$$

Where i, j, k, l → 1,2,3 and the anisotropic (orthotropic) elastic tensor of FCC single crystal nickel is (units: GPa);-

$$\begin{bmatrix} C_{11} & C_{12} & C_{12} & 0 & 0 & 0 \\ C_{12} & C_{11} & C_{12} & 0 & 0 & 0 \\ C_{12} & C_{12} & C_{11} & 0 & 0 & 0 \\ 0 & 0 & 0 & C_{44} & 0 & 0 \\ 0 & 0 & 0 & 0 & C_{44} & 0 \\ 0 & 0 & 0 & 0 & 0 & C_{44} \end{bmatrix} = \begin{bmatrix} 247 & 147 & 147 & 0 & 0 & 0 \\ 147 & 247 & 147 & 0 & 0 & 0 \\ 147 & 147 & 247 & 0 & 0 & 0 \\ 0 & 0 & 0 & 125 & 0 & 0 \\ 0 & 0 & 0 & 0 & 125 & 0 \\ 0 & 0 & 0 & 0 & 0 & 125 \end{bmatrix} \tag{30}$$

Hydrogen diffusion without the effect of stress in the FCC single crystal is isotropic with one independent diffusion material property [48]. The lattice hydrogen diffusion properties used in the bi-crystal model is $D=3.52\times10^{-10}$ cm^2/s [4]. In the bi-crystal model the hydrogen enters into the material from the left hand side of the bi-crystal specimen and there is no initial hydrogen present in the material. Different hydrogen diffusion co-efficients are required along the grain boundary. A few authors have experimentally observed faster diffusion of hydrogen along the grain boundary when compared to the lattice in FCC nickel material [4, 51-52]. In this work the specific hydrogen diffusion properties along grain

boundaries have been assigned the value Dgb=2.05×10^{-8} cm^2/s (i.e. diffusivity of grain boundary) [4]. A 3D bi-crystal model is used with two cubic single crystals one in the bottom named crystal1 (i.e. fixed crystal) and one at the top named crystal2 (i.e. tilted crystal) with a grain boundary as the interface between them is shown in Fig. 1(a). Fig. 1(a) illustrates the geometry and boundary conditions of the 3D bi-crystal model of nickel. Fig. 1(b) shows the geometric representation of a TGB in the bi-crystal model. The crystal and grain boundaries are separated by geometrical lines with the "grain boundary affected zone" (GBAZ) represented by geometrically separated lines either side of the grain boundary lines to enable assignment of specific properties for grain boundaries within this region as shown in Fig. 1 (c). The dimension of GBAZ is assumed to be 5nm (i.e the thickness of GB). In this way the specific diffusion properties of grain boundaries are accounted for. The procedures to develop grain, GBAZ and assign diffusion properties are described by Jothi and co-authors [2]. A uniform tensile load is applied to the bi-crystal model in the y-direction as shown in Fig. 1(a). A mesh convergence study was then performed in ABAQUS to eliminate mesh sensitivity and to ensure the precision of the analysis. The number of elements used was based on the mesh convergence study. A very fine mesh is used in the microstructural meso-scale model to accurately capture gradients of stress and hydrogen concentration in the crystal and grain boundaries. Each crystal was divided into 250000 solid linear elements in the bi-crystal model. The total number of nodes and elements in bi-crystal models of various misorientation of GB are 513525 and 512000 respectively. Fig.1 (c) shows a close-up view of grains and the GBAZ meshing. Anisotropic cubic elasticity was considered for each grain for when modelling the structural elastic response of the nickel by assigning various GB misorientation angles 0°≤ θ ≤ 90°. The analysis consists of a mechanical structural analysis followed by a hydrogen diffusion analysis of both bi-crystal models. Initially, the mechanical responses of the microstructural model with the detailed microstructural local stresses near the grain boundary are captured using the initial mechanical stress analysis. The calculated hydrostatic stresses from the stress analysis are saved as nodal averaged values. During the course of hydrogen diffusion analysis these hydrostatic stresses, which provide the driving force for the hydrogen diffusion, are obtained by reading from a structural analysis results file.

3. Results and discussions

3.1 *Effects of TGB misorientation angle on hydrostatic stress in bi-crystal model:*

The bi-crystal model comprises crystal1 and crystal2 separated by a GB and GBAZ. The GBAZ simulates hydrogen diffusion along the GB. The lattice misfit between the crystals accommodates the GB misorientation. The orientation of crystal1 is fixed and the orientation of crystal2 is tilted along the traction direction to form geometric TGBs for various misorientation angles 0°, 5°, 15°, 30°, 35°, 40°, 45°, 60°, 75°, 85° and 90° as shown in Fig. 1(b). Figs. 2(a), (b) and (c) shows the calculated microscopic hydrostatic stress (σ_h) normalized by the applied uniform macroscopic stress (σ_0) parallel to the traction direction for various TGB misorientation angles along the paths x1, x2 and x3 respectively. In figs. 2(a), (b) and (c) the normalized distance at a point is defined as the y-coordinate divided by the total height (2h) of the crystal as shown in figure1, assuming the origin is at the bottom edge of the bi-crystal. This, if the normalized distance at a point is zero then it is at the extreme bottom side of the bi-crystal, a value of 0.5 is the centre of the bi-crystal and if the normalized distance value is 1 then the position is at extreme top of the bi-crystal along y-direction, irrespective of the actual width of the crystal. The Path x1 is near the left hand corner of the crystals, path x2 is in the middle of the crystals and path x3 is near the right hand corner of the crystals as shown in Fig. 1(a). The path x1 is plotted along the blue arrow line on the surface of bi-crystal nickel as shown in fig.2 (a) in order to understand the influence of the boundary on various misorientation angles. The path x2 is plotted along the blue arrow line on the surface of bi-crystal nickel as shown in fig.2 (b) (i.e. middle of the nickel bi-crystal) in order to investigate the influence of misorientation angles under externally applied stress conditions at a region away from the boundary conditions applied at the left hand side of the mesh along path x1. Similarly, path x3 is plotted along the blue arrow line on the surface of bi-crystal nickel as shown in fig.2 (c) (i.e the side of the mesh opposite to the path x1) in order to investigate the influence of misorientation angle on hydrostatic stress developed under externally applied stress conditions away from the boundary conditions applied at the left hand side of the mesh along path x1 and to investigate the variation of the developed hydrostatic stress inside the crystal and grain boundary due to the deformation constraint caused by the adjutant crystal by misorientation angle. The computed results in Fig. 2 show the hydrostatic stress distribution is uniform and homogenous for TGB misorientation 0° and 90° for each path. In contrast the hydrostatic stress distribution tends to

be heterogeneous and nonuniform between crystals for TGB misorientation angles 15°, 30°, 35°, 40°, 45°, 60° and 75° (i.e. orientations $> 0°$ and $< 90°$) .

Fig. 2(a) shows the influence of misorientation angles on hydrostatic stress along the path x1. The path x1 is plotted in order to understand the influence of the boundary on various misorientation angles. The normalized hydrostatic stress distribution between the crystals tends to be smaller near the traction side and increase moving towards the TGB attaining a maximum value close to the TGB along path x1 for misorientations between 15° and 45°. In reality, as opposed to the numerical model, the difference in the mechanical elastic properties of crystal1 and crystal2 due to misorientation would affect dislocations near the TGB due to the applied load. Varying hydrostatic stresses along the TGB and near to TGB arise depending on the misorientation angles. The maximum accumulated local hydrostatic stress values on the TGB are tensile and 0.8 times of the applied uniform tensile stress for a misorientation angle of 30°. For misorientation angles greater than 45° and less than 90° the hydrostatic stress values between the crystals start to decrease along the path x1 when moving from the traction side towards the TGB reaching a minimum close to the TGB. The minimum local accumulated hydrostatic stress values on the boundary are compressive with the highest normalized compressive stresses less than 0.2 normalized stresses observed in the model with a misorientation of 60°. The compressive stresses are due to the effects of boundary and misorientation angle. *These results show that the localized hydrostatic stress concentrations inside the crystals and near to the TGB are governed primarily by the TGB misorientation.*

Fig. 2(b) shows the normalised hydrostatic stress distribution between the crystals and TGB along the path x2 for various misorientation angles. Path x2 was plotted along the blue arrow line on the surface of bi-crystal nickel as shown in fig.2 (b) (i.e. middle of the nickel bi-crystal). The paths x2 results are plotted in order to understand the influence of misorientation angles on hydrostatic stresses without the effects of boundaries. The maximum normalized hydrostatic stress value is observed on the fixed crystal near to the TGB for misorientation angle 45° and the minimum normalized hydrostatic stress value is observed near to the TGB on the tilted crystal of the bi-crystal model with 45° misorientation angle. The minimum hydrostatic stress value is observed on the crystal1 near to the TGB with misorientation angle 75° and the maximum hydrostatic stress value is observed on the crystal2 near the TGB of the model with misorientation angle 15°. *The highest accumulation of hydrostatic stress concentrations are near to the TGB on the fixed crystal (i.e. Crystal1)*

and lowest values of local hydrostatic stress concentrations are observed near to the TGB on the rotated crystal (i.e. crystal2) along path x2.

Fig. 2(c) shows the normalised hydrostatic stress distribution between the crystals and boundary along the path x3 for various TGB misorientations. Higher stress gradients are observed near the GB. *Low values of localized hydrostatic stress concentration are observed near the boundary on the fixed crystal and high values of localized hydrostatic stress concentration are observed near the boundary on the tilted crystal.* The minimum localized hydrostatic stress values are observed on the fixed crystal near the boundary for misorientation angles 30° and 35° and the maximum localized hydrostatic stress value is observed in crystal2 along the TGB of misorientation angle 60°. However, the difference between the maximum and minimum values of localized hydrostatic stress concentration along the TGB are observed to be highest for the misorientation angles of 45° and 40° and the lowest differences are observed for misorientation angles of 15° and 75°.

3.2 *Effects of boundary condition and misorientation angle on hydrostatic stress in the bi-crystal model:*

Figs. 3(a) and (b) show the normalized hydrostatic stress distribution along the path near to the tilt boundary on the GBAZ of crystal1 (fixed crystal) and crystal2 (tilted crystal) perpendicular to the traction direction for various TGB misorientation angles. This shows the influence of TGB misorientation angles due to applied boundary conditions. The normalized hydrostatic stresses accumulated near to the tilt boundary of crystal1 and crystal2 for misorientation angles in the range $0°<\theta<45°$ are in the form of tensile stresses with values higher than those obtained with misorientation angles of 0° and 90°. The normalized hydrostatic stress accumulated near the tilt boundary on the left hand side of crystal1 and crystal2 for a misorientation angle 85° are in the form of tensile stresses with (i) lower values than those obtained with misorientation angles 0° and 90° and (ii) higher values on the right hand side of crystal1 and crystal2 (but still < 0.4). The normalized hydrostatic stresses accumulated near the tilt boundary on the left side of crystal1 and crystal2 for GB misorientation angles $45°<\theta<85°$ are in the form of compressive stresses due to the applied boundary condition whereas the right side of crystal1 and crystal2 are in the form of tensile stresses, these tensile normalized hydrostatic stresses values are not higher than 0.5. *These results show that the areas closest to the left corner of the tilt boundary are accumulating both the tensile and compressive localized hydrostatic stress concentrations due to the effect of the applied boundary condition. Thus applied boundary conditions with the deformation*

constrained by the neighbouring crystal orientations also plays an important role in stress distributions related to TGB misorientation angle. These results also suggest that the generated hydrostatic stresses are low on misorientation angles 45°<θ<90° when compared to misorientation angles 0°<θ<45°. The misorientation angles ranging between 45°<θ<85° generate compressive stresses which may increase the resistance to hydrogen embrittlement as explained by Takakuwa al, [49] who concluded that the compressive stresses may provide resistance to hydrogen embrittlement. The highest normalized hydrostatic tensile stress with a value of 0.9 is found in crystal1 (fixed crystal) for the TGB misorientation angle 30° and the highest normalized hydrostatic compressive stress with a value of -0.3 is found in crystal2 (tilted crystal) for the misorientation angle 60°.

3.3 Effects of GB misorientation on normal stress in the bi-crystal model:

Figs. 4(a),(b) and (c) show the microscopic normal stress (σ_{22}) normalized by the applied uniform macroscopic stress (σ_0) parallel to the traction direction along the paths x1, x2 and x3 respectively for various TGB misorientation angles. The high and low normalized normal stresses accumulate near the tilt boundary and the highest tensile stress with a value of 1.9 is found on the left hand side of the crystals near the tilt boundary with misorientation angle 30°. The highest compressive stress is found on the left hand side of the crystals near the tilt boundary with a value of -0.6. The left side region in the bi-crystal model, near the tilt boundary, is where the highest normalized normal stresses are found for TGB misorientation angles 0°<θ<45° while the lowest normalized normal stresses are found for TGB misorientation angles 45°<θ<90°. The right hand side of the bi-crystal model near the tilt boundary is where the highest and lowest normalized normal stresses are found for TGB misorientation angles 45°<θ<90°. *These results suggest that the tensile, compressive and highest/lowest values of normal stresses accumulate near the tilt boundary with values dependent on TGB misorientation angles. Since hydrostatic stress depends on the normal stress as shown in Eq.(7), then highest and lowest tensile and compressive hydrostatic stresses accumulate near the tilt boundary with values also dependent on misorientation angle. Thus stress gradients near TGBs are dependent on misorientation angles.*

3.4 Effects of GB misorientation on von Mises stress and shear strain distribution in the bi-crystal model:

Fig. 5 shows the maximum local normal stress, maximum hydrostatic stress and maximum von Mises stress normalized by the applied uniform macroscopic stress for various TGB misorientation angles. The values of the maximum normalized normal stress and the

maximum normalized von Mises stress vary approximately in the range $1 - 1.8$ for various TGB misorientation angles. The values are 1.0 for TGB misorientations 0° and 90° due to zero dilatational mismatches produced along the TGB. Values greater than 1.0 are for misorientation angles $0° < \theta < 90°$ with high magnitudes of stress observed for misorientation angles $15° < \theta < 45°$. High stresses appear near GBs. Figs. 6 (a), (b) and (c) show the local shear strain (ε_{12}) normalized by applied strain ($\varepsilon_0 = L_0/L$) along the paths x1, x2 and x3 parallel to the traction direction for various TGB misorientation angles. The magnitudes of shear stress appear low in the fixed crystal and high in the tilted crystal. The shear strain jumps from lower to higher values near the TGB with the highest shear strain appearing along the TGB. *These results suggest that the local stress and strain distribution in the nickel bi-crystal case are governed primarily by the TGB misorientation angles.*

3.5   Effects of GB misorientation on hydrogen distribution in the bi-crystal model:

Fig. 7 shows the normalized hydrogen concentration along the normalized path x1 parallel to the traction direction for various TGB misorientation angles. The figure shows higher hydrogen concentration gradients along the TGB. In the numerical model this effect is explained by the fact that i) the elastic constants in the modelled crystals are a function of orientation, ii) these differences directly affect the calculated hydrostatic stresses which iii) directly affect diffusion and the evolution of the hydrogen concentration field. The effect in real material, as opposed to the numerical model, is the same but the explanation would proceed along the following lines, i) the overall uniform applied elastic stress on the bi-crystal generates dislocations along TGB due to the dilatational mismatch produced by differences in the mechanical responses arising from the differences in anisotropic elasticity between tilted crystal and fixed crystal ii) the dislocations developed along TGB act as hydrogen trap sites which segregate and accumulate hydrogen concentrations in the form clustered atomic hydrogens along TGB iii) where the amount of dislocation generation is governed by the GB misorientation angle and the variation in the amount of dislocations generated depends on the misorientation angle between the two adjacent crystals.

The hydrogen concentrations are heterogeneously distributed in the bi-crystal nickel model for TGB misorientations $0° < \theta < 90°$ due to the change in stress gradients i.e. heterogeneous distribution of normalised hydrostatic stresses (σ_h/σ_0) whose values are greater or lower than 0.33 and normalised normal stress (σ_n/σ_0) greater or less than unity. In contrast the hydrogen concentration is homogenously distributed for GB misorientations 0° and 90° because the homogeneous distribution of normalised hydrostatic stresses (σ_h/σ_0) are equal to

0.33 and the normalised normal stress (σ_n/σ_0) are equal to 1. The normal hydrostatic tensile and compressive stresses are acting as the driving forces for higher and lower local accumulations of hydrogen respectively. The hydrogen concentrations near the TGB can be higher or lower depending on the misorientation angle. The accumulated hydrogen concentrations are higher near the TGB for misorientation angles $0°<\theta<45°$ and lower for misorientation angles $45°<\theta<90°$. Increased hydrogen concentrations along the TGB are observed for tensile normalised normal stress and normalised hydrostatic stresses (σ_h/σ_0) whose values are greater than 1 and 0.33 respectively. Lower accumulations of hydrogen along the TGB misorientation are observed with compressive normalised normal stress and normalised hydrostatic stresses whose values are less than 1 and 0.33 respectively. Tensile stresses with higher stress gradients segregate higher concentration of hydrogen. Higher accumulation of hydrogen concentration are observed with misorientation angles $0°<\theta<45°$ due to high tensile stresses acting on these misorientation angles. Lower segregations of hydrogen concentration are observed on misorientation angles $45°<\theta<90°$ due to high compressive stresses. This numerical prediction suggests that TGBs act as trap sites as well as non-trap sites depending on the type of stresses acting on the TGB i.e. tensile or compressive.

Fig. 8 shows the normalised hydrogen concentration along the normalized path x2 parallel to the traction direction for various GB misorientations after normalized time. Figs. 9 and 10 show the normalized hydrogen concentration along the normalized path near the TGB on crystal1 (i.e. fixed crystal) and crystal2 (tilted crystal) perpendicular to the traction direction for various misorientation angles respectively. Fig. 11 shows the corresponding plot of normalised hydrogen concentration for various GB misorientations.

In a real material the amount of hydrogen traps would increase along the TGB as the tensile stress increases. An increase in dilatational mismatch between crystals increases the tensile stress. The amount of hydrogen traps would correspondingly decrease along a TGB as the compressive stress increases due to a decrease in the dilatational mismatch between crystals.

In the model case Fig. 12 shows the maximum normalized hydrogen concentration as a function of TGB misorientation angles after various normalized times. The maximum hydrogen segregations increase as the TGB misorientation angle increases above 0° attaining a maximum for the TGB misorientation angle of 35° then decreasing and attaining a steady

state after the TGB misorientation angle of 85°. Thus the model predicts maximum highly segregated hydrogen concentrations are found on TGB misorientation angles in the range $15° < \theta < 45°$.

The results of numerical modelling in this paper indicate that the TGB misorientation angle affects the followings factors: neighbouring crystal boundary conditions, changes in stress gradients, types of stress developed (i.e. tensile/ compressive) depending on the applied boundary condition and neighbouring crystal orientations. The effect of stress induced hydrogen diffusion in the meso-scale bi-crystal nickel model would indicate that the TGB misorientation angles are one of the key factors that significantly influence hydrostatic stress, normal stress, strains and hydrogen distributions in nickel. This result illuminates the problem of how TGB misorientation angles influence hydrogen segregation and trapping in bi-crystal nickel specimens and the effects of TGB misorientation on stress induced hydrogen evolution. This knowledge could be beneficial for optimization of TGB misorientations in materials in order to reduce hydrogen traps and segregations sites which would lead to improvements in resistance to hydrogen induced intergranular cracking and hydrogen embrittlement.

4. Conclusion

In this present study a numerical tool was developed to investigate the effects of TGB misorientation angle on stress induced hydrogen distributions in bi-crystal nickel. A computational finite element analyses based on GB engineering was employed. Initially mechanical stress analyses were executed to appraise the dilatational stress distribution, normal stress distribution, and shear strains distributions. Subsequently coupled stress-assisted mass diffusion modelling was performed in order to quantify the influence of TGB misorientation angles on the local stress, strain and hydrogen distributions in bi-crystal nickel. Such an approach could aid design and optimization of materials in order to identify the conditions that maximize resistance to hydrogen embrittlement and hydrogen induced intergranular cracking. This approach is not necessarily only applicable to nickel-hydrogen system but could also be used for evaluating environmental cracking and intergranular cracking due to other stress induced atomic impurity diffusion (e.g. boron, oxygen, sulphur etc.) in bi-crystals and polycrystalline metallic materials. The results are summarized as follows:

- In the mechanical stress analysis the induced hydrostatic stress, Von Mises stress, normal stress, and shear strain distributions differ depending on the TGB misorientation angles along the direction of the applied load. This is produced in the model by the dilatational mismatch along the TGB being modelled as a difference in anisotropic elasticity between two individual crystals in bi-crystal nickel.

- In the stress-assisted hydrogen diffusion analysis the dilatational stresses act as a driving force during the evolution of the hydrogen distribution. The evolving hydrogen distribution varies depending on the TGB misorientation angles.

- The stresses and hydrogen distributions in bi-crystal nickel are homogenous for TGB misorientation angles of 0° and 90° and strongly heterogeneous for TGB misorientation angles $0°<\theta<90°$ under uniform applied mechanical loading.

- The types of stress produced (i.e. tensile or compressive) depend on the applied boundary conditions due to deformation constraints arising from crystal misorientations.

- The model results are in agreement with experimental observations where experimentally it is observed that a large amount of hydrogen is trapped in regions under tensile stress because of a local increase in dislocations. Correspondingly, hydrogen trapping is reduced in regions of compressive stress.

- Increasing dilatational mismatch along TGBs and near to TGBs increases the hydrostatic stress based on misorientation angles which leads to increased hydrogen segregation.

- Decreasing dilatational mismatch decreases hydrostatic stress gradients based on misorientation angles which leads to decreased amounts of hydrogen segregation.

- The maximum segregation of hydrogen concentration depends on the TGB misorientation angle. The maximum segregation of hydrogen tends to increase for TGB misorientation angles greater than 0° attaining a maximum for a TGB misorientation angle of 35° subsequently decreasing for TGB misorientation angles $35°<\theta<90°$ in the bi-crystal model.

- A numerical modelling framework has been demonstrated that allows consideration of grain boundary misorientation angles for studying hydrogen segregation and thus intergranular hydrogen embrittlement (associated with induced tensile stresses) and also the suppression of intergranular hydrogen embrittlement (associated with induced compressive stresses).

- The numerical model predicts maximum hydrogen concentrations are accumulated on the TGB with misorientation angles ranging between $15°<\theta<45°$ and minimum hydrogen concentrations are accumulated on the TGB with misorientation angles ranging between $0°<\theta<5°$ and $75°<\theta<90°$. The model therefore predicts that TGBs with misorientation angles ranging between $0°<\theta<5°$ and $75°<\theta<90°$ are the preferred microstructures of bi-crystal nickel.

- This technique can be used to investigate the importance of GB engineering for designing and optimizing bi-crystal and polycrystalline materials to help decrease hydrogen segregation arising from TGB misorientation angles for specific boundary conditions.

Acknowledgements

References:

[1] M.L. Martin, B.P. Somerday, R.O. Ritchie, P. Sofronis, I.M. Robertson, Hydrogen-induced intergranular failure in nickel revisited, Acta Materialia 2012; 60:2739-2745.
[2] S. Jothi, T.N. Croft, S.G.R .Brown, E.A. de Souza Neto, Finite element microstructural homogenization techniques and intergranular, intergranular microstructural effects on effective diffusion coefficient of heterogeneous polycrystalline composite media, Composite Structures 2014;108:555-564.
[3] R.M. Latanision, H. Opperhauser.Jr, Further observations on the effect of grain boundary segregation in the hydrogen embrittlement of nickel, Metallurgical Transactions A 1975;6A:233-234.
[4] T. Tsuru, R.M. Latanision, Grain boundary transport of hydrogen in nickel, Scripta Metall 1982;16:575-578.
[5] L.C. Lim, T. Watanabe, Grain boundary character distribution controlled toughness of polycrystals - a two dimensional model, Scripta Metall 1989; 23:489-495.
[6] T. Watanabe, Structural effects on grain boundary segregation, hardening and fracture, Journal de Physique, 1985;46 C4:555-564.
[7] T. Watanabe, T. Murakami and S. Karashima, Misorientation dependence of grain boundary segregation, 1978;12:361-365.

[8] S. Kobayashi, T. Maruyama, S. Tsurekawa, T. Watanabe, Grain boundary engineering based on fractal analysis for control of segregation induced intergranular brittle fracture in polycrystalline nickel, Acta Materialia 2012;60:6200-6212.

[9] T. Watanabe, An approach to grain boundary design for strong and ductile materials, Res. Mechanica, 1984;11:47-84.

[10] L.C. Lim, T. Watanabe, Fracture toughness and brittle-ductile transition controlled by grain boundary character distribution (GBCD) in polycrystals, Acta Metallurgica et Materialia 1990;38:2507-2516.

[11] G. Palumbo, K.T. Aust, Structure-dependence of intergranular corrosion in high purity nickel, Acta Met Mater 1990;38:2343-2352.

[12] G. Palumbo, P.J. King, K.T. Aust, U. Erb, P.C.Lichtenberger, Grain boundary design and control for intergranular stress corrosion resistance, Scripta Metallurgica et Materialia 1991;25:1775-1780.

[13] P. Lin, G. Palumbo, U. Erb, K.T. Aust, Influence of grain boundary character distribution on sensitization and intergranular corrosion of alloy 600, Scripta Metallurgica et Materialia 1995;33:1387-1392.

[14] E.M. Lehockey, D. Limoges, G. Palimbo, J. Sklarchuk, K. Tomantschger, A. Vincze, On improving the corrosion and growth resistance of positive Pb-acid battery grids by grain boundary engineering, 1999;78:79-83.

[15] C. Cheung, U. Erb, Application of grain boundary engineering concept to alleviate intergranular cracking in Alloys 600 and 690, Materials science and Engineering:A 1994;185:39-43.

[16] E.M. Lehockey, G. Palumbo, On the creep behaviour of grain boundary engineered nickel 1, Materials Science and Engineering: A 1997; 237:168-172.

[17] D.C. Crawford, G.S. Was, The role of grain boundary misorientation in intergranular cracking of Ni-16Cr-9Fe in 360°C argon and high purity water, Metall. Mater. Trans.A, 1992; 23:1195-1206.

[18] M.A. Arafin, J.A. Szpunar, A new understanding of intergranular stress corrosion cracking resistance of pipeline steel through grain boundary character and crystallographic texture studies, Corrosion Science 2009;51:119-128.

[19] C.A. Schuh,M. Kumar,W.E. King, Analysis of grain boundary networks and their evolution during grain boundary engineering, Acta Materialia 2003;51:687-700.

[20] V. Randle, twinning-related grain boundary engineering, Acta Materialia 2004; 52:4067-4081.

[21] G. Palumbo, F. Gonzalez, A.M. Brennenstuhl, U. Erb, W. Shmayda, P.C. Lichtenberger, In-situ nuclear steam generator repair using electrodeposited nanocrystalline nickel, Nanostructured Materials 1997;9:737-746

[22] A.W. Thompson, Effect of grain size on work hardening in nickel, Acta Metallurgica 1997; 25:83-86.

[23] R.A. Jago, N. Hansen, Grain size effects in the deformation of polycrystalline iron, Acta Metallurgica 1986;34:1711-1720.

[24] L. St-Pierre, E. Heripre, M. Dexet, J. Crepin, G. Bertolino, N. Bilger, 3D simulations of microstructure and comparison with experimental microstructure coming from O.I.M analysis, International Journal of Plasticity 2008;24:1516-1532.

[25] Y. Zhao, R. Tryon, Automatic 3-D simulation and micro-stress distribution of polycrystalline metallic materials, Computational Methods in Applied Mechanics and Engineering 2004;193:3919-3934.

[26] T.J. Turner, P.A. Shade, J.C. Schuren, M.A. Goeber, The influence of microstructure on surface strain distributions in a nickel micro-tension specimen, Modelling and Simulation in Materials Science and Engineering 2012;21:015002 (23pp).

[27] D.H. Lassila, H. Birnbaum, The effect of diffusive hydrogen segregation on fracture of polycrystalline nickel, Acta Metallurgica, 1986; 34:1237-1243.

[28] H. Fukushima, H.K. Birnbaum, Surface and grain boundary segregation of deuterium in nickel, Acts Metallurgica, 1984; 32:851-859.

[29] D. Turnbull, R.E. Hoffman, The effect of relative crystal and boundary orientations on gran boundary diffusion rates, Acta Metallurgica 1954; 2:419-426.

[30] C. Herizg, S.V. Divinski, Grain boundary diffusion in Metals: Recent Developments, Materials Transactions 2003;44:14-27.

[31] V. Randle, Microtexture determination and its applications, Bourne Press 1992.

[32] V. Randle, The role of the Coincidence Site Lattice in Grain boundary engineering, The University Press 1996.

[33] S.R. Arwade, M. Grigoriu, Probabilistic model for polycrystalline microstructures with application to intergranular fracture, Journal of Engineering mechanics 2004; 997-1005.

[34] S. Ghosh, S. Moorthy, Three dimensional Voronoi cell finite element model for microstructures with ellipsoidal heterogeneities, Computational Mechanics. 2004; 34:510-531.

[35] A.A. Elvin, S. Shyam Sunder, Microcracking due to grain boundary sliding in polycrystalline ice under uniaxial compression, Acta Mater. 1996; 44:43-56.

[36] C.R. Chen, S.X. Li, J.L. Wen, W.P. Jia, Finite element analysis about effects of stiffness distribution on stresses and elastic strain energy near the triple junction in a tricrystal, Materials Science and Engineering 2000;A282:170-176.

[37] S. Jothi, T.N. Croft, S.G.R. Brown, E.A. de Souza Neto, Multiscale modelling of hydrogen embrittlement in polycrystalline materials. In: Proc. 12thESIA Conference 2013.

[38] S. Jothi, T.N. Croft, S.G.R. Brown, E.A. de Souza Neto, A multiscale chemo-mechanical model of hydrogen embrittlement in polycrystalline nickel. In: Proc. SteelHydrogen Conference 2014.

[39] T.C.T. Ting, Anisotropic elasticity: Theory and Applications, Oxford: Oxford University Press 1996.

[40] J.M.J. den Toonder, J.A.W. van Dommelen and F.P.T. Baaijens, The relation between single crystal elasticity and the effective elastic behaviour of polycrystalline materials: theory, measurement and computation, Modelling Simul. Mater.Sci. Eng. 1999;7:909-928.

[41] S. Li, J. Zhou, L. Ma, N. Xu, R. Zhu, X. He, Continuum level simulation on the deformation behaviour of nanocrystalline nickel, Computational Materials Science 2009; 45:390-397.

[42] J.F. Nye, Physical properties of Crystals, Oxford: Clarendon 1985.

[43] F. Roters, P. Eisenlohr, L. Hantcherli, D.D. Tjahjanto, T.R. Bieler, D. Raabe, Overview of constitutive laws, kinematics, homogenization and multiscale methods in crystal plasticity finite-element modelling: Theory, experiments, applications, Act Materialia 2010;58:1152-1211.

[44] C.S. Nichols, R.F. Cook, D.R. Clarke, D.A. Smith, Alternative length scales for polycrystalline materials, Acta Metall. Mater. 1991; 39:1657-1665.

[45] O. Diard, S. Lecercq, G. Rousselier, G. Cailetaud, Evaluation of finite element based analysis of 3D multicrystalline aggregates plasticity: application to crystal plasticity model identification and the study of stress and strain fields near grain boundaries, International Journal of plasticity 2005; 21:691-722.

[46] M. Meyers and K. Chawlu, Mechanical behaviour of materials, Second Edition, Cambridge University Press 2009.

[47]   F. Barbe, S. Forest, G. Cailetaud, Intergranular and intragranular behaviour of polycrystalline aggregates. Part 2. Results, International Journal of Plasticity 2001;17:537-563

[48]   H. Mehrer, Diffusion in solids: Fundamentals, Methods, Materials, Diffusion-Controlled processes, Springer 2007.

[49]   O. Takakuwa, M. Nishikawa, H. Soyama, Numerical simulations of the effects of residual stress on the concentration of hydrogen around a crack tip, Surface & Coating Technology 2012;206:2892-2898.

[50]   T. Kitamura, T. Sumigawa, K. Ohishi, Slip behaviour and local stress near grain boundary in high-cycle fatigue of copper polycrystal, JSME international journal 2004;47:92-97.

[51]   G. Palumbo, D.M. Doyle, A.M. El-Sherik, U. Erb, K.T. Aust, Intercrystalline hydrogen diffusion transport in nanocrystalline nickel, Scripta Metall. 1991;25:679-684.

[52]   T.M. Harris, R.M. Latanision, Grain boundary diffusion of hydrogen in nickel, Metallurgical Transactions A, 1991; 22A: 351-355.

[53]   A. Turnbull, Modelling of environment assisted cracking, Corrosion Science 1993; 34:921-960.

[54]   A.H.M. Krom, R.W.J. Koers, A. Bakker, Hydrogen transport near a blunting crack tip, J Mech Phys Solids, 1999; 47:971-992.

Influence of grain boundary misorientation on hydrogen embrittlement in bi-crystal nickel.

*S. Jothi, T. N. Croft, S. G. R. Brown

College of Engineering, Swansea University, Singleton Park, Swansea SA2 8PP, UK
*S.Jothi@swansea.ac.uk
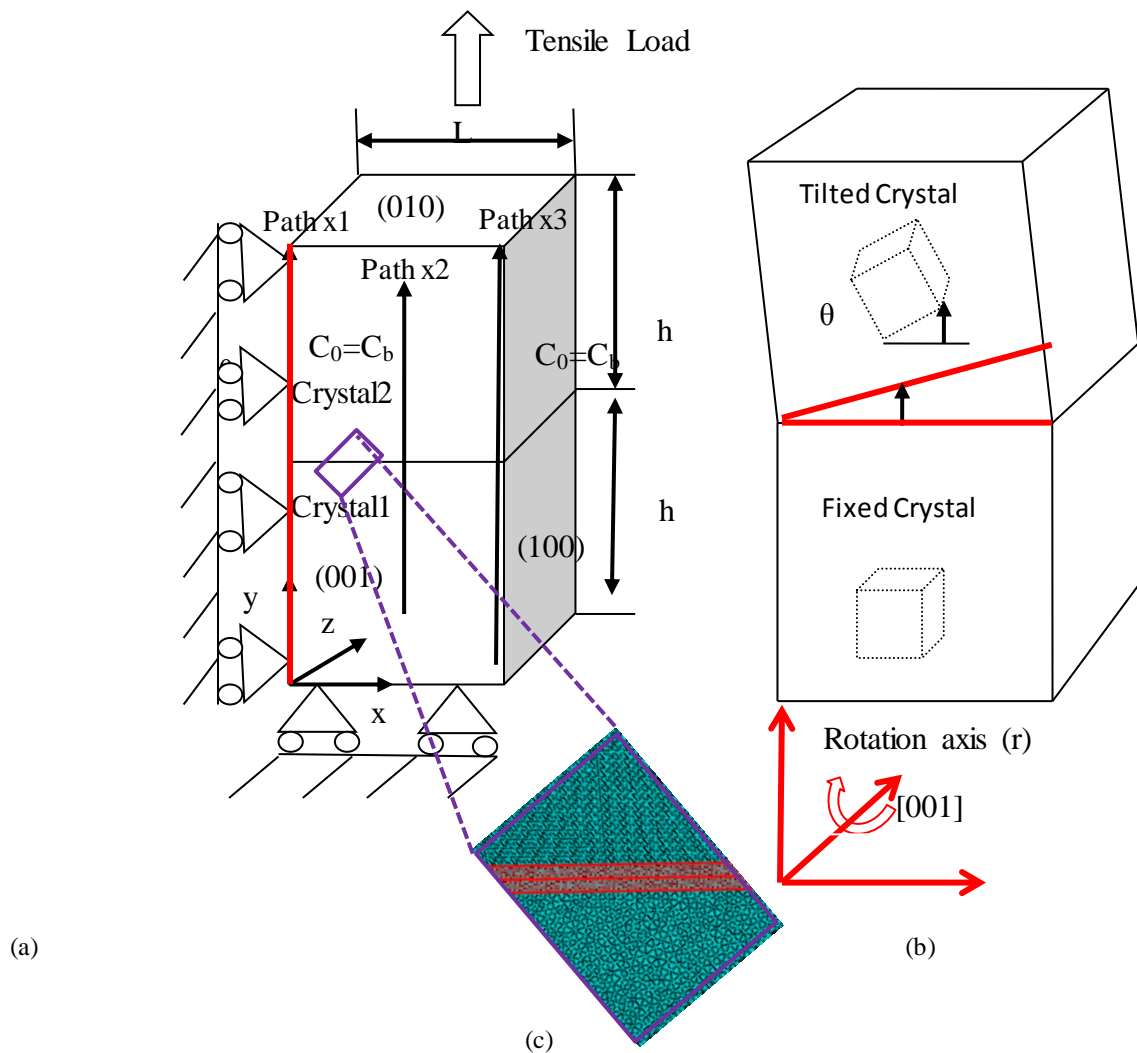
Fig. 1(a) Shows the geometry and boundary conditions of the Bi-Crystal model and the path x1, x2, x3 along the traction direction (b) TGB based on fixed and tilted crystal to form various misorientation angles (θ) (0°, 5°,15°, 30°, 35°, 45°, 60°, 75°, 85°, 90) to the rotation axis [001 and (c) close-up view of FE mesh of crystal (blue colour) and grain boundary affected zone (red colour).

Tilt Grain Boundary
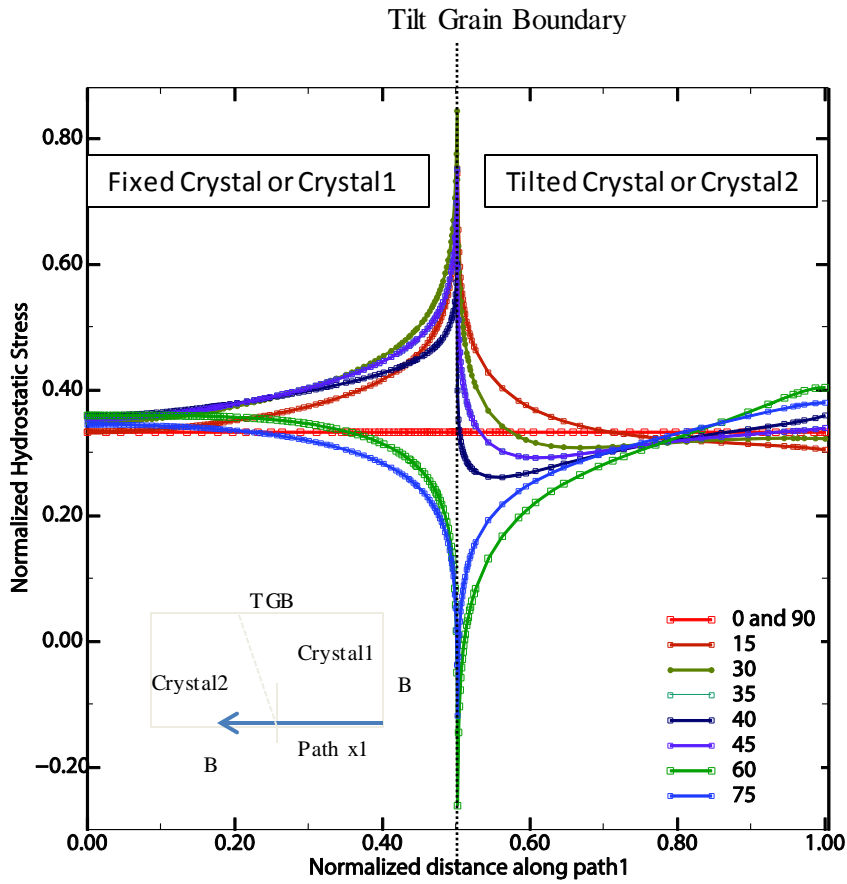
Fig. 2(a) Shows the normalized hydrostatic stress (σ_H/σ_0) due to the boundary effect along the normalized path x1 (y/h) parallel to the traction direction for various misorientation angles in degrees.

TGB
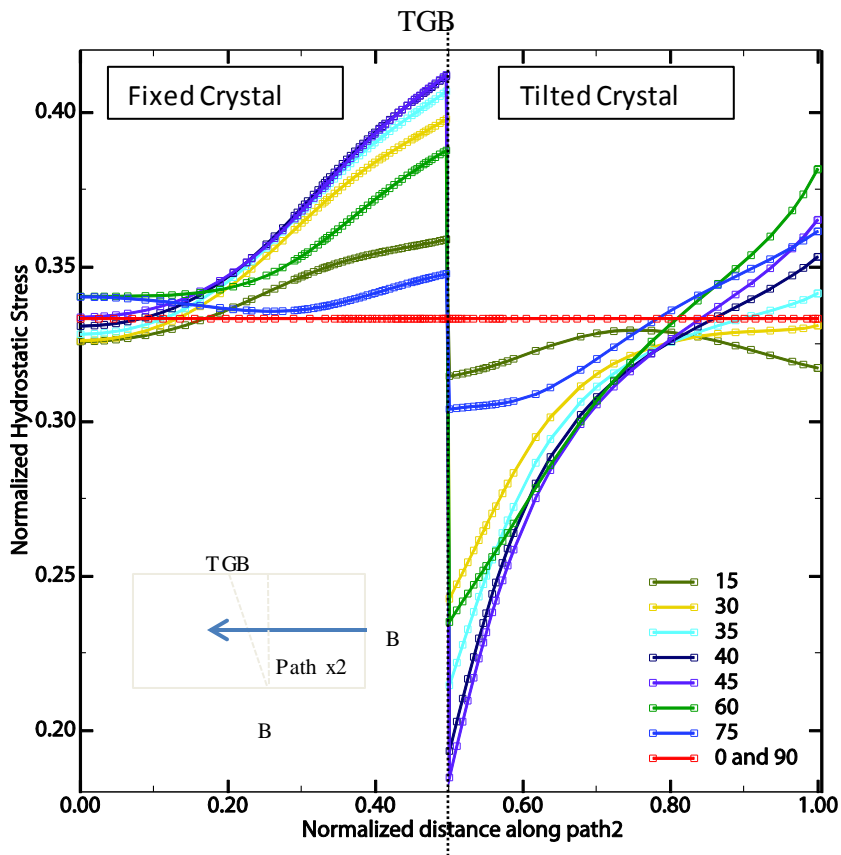
Fig. 2(b) Shows the normalized hydrostatic pressure (σ_H/σ_0) along the normalized path x2 (y/h) parallel to the traction direction for various misorientation angles in degrees.
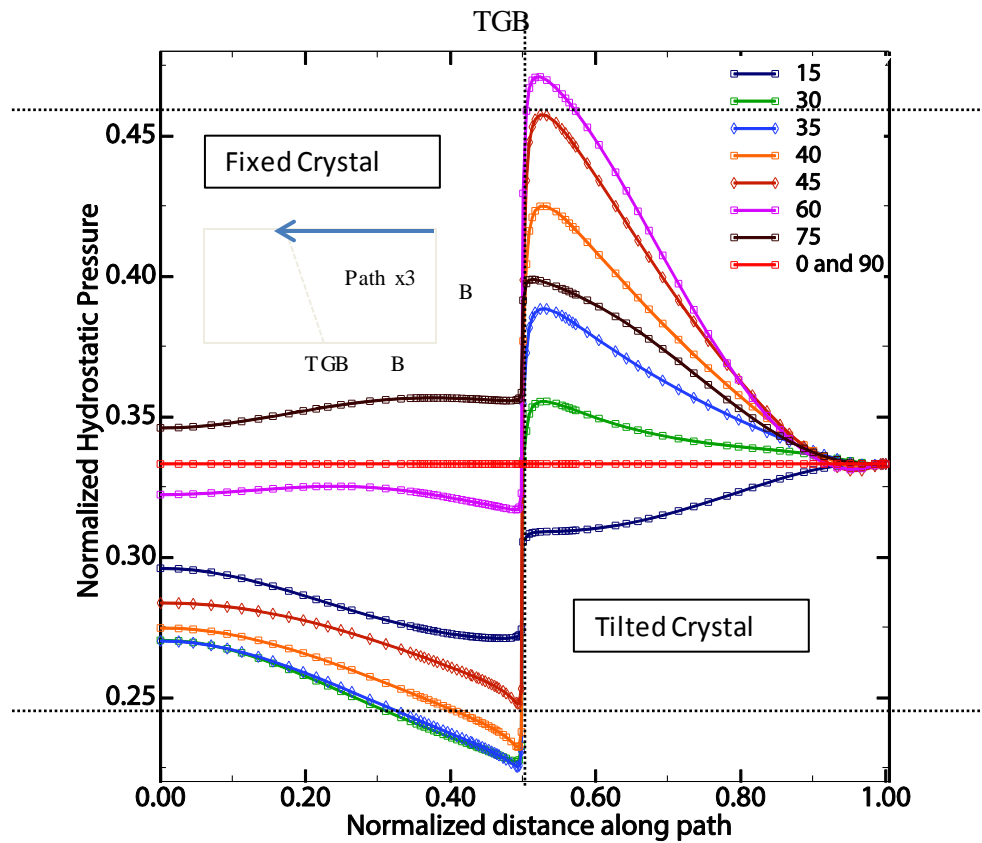
Fig. 2(c) shows the normalized hydrostatic pressure (σ_H/σ_0) along the normalized path x3 (y/h) parallel to the traction direction for various misorientation angles in degrees.
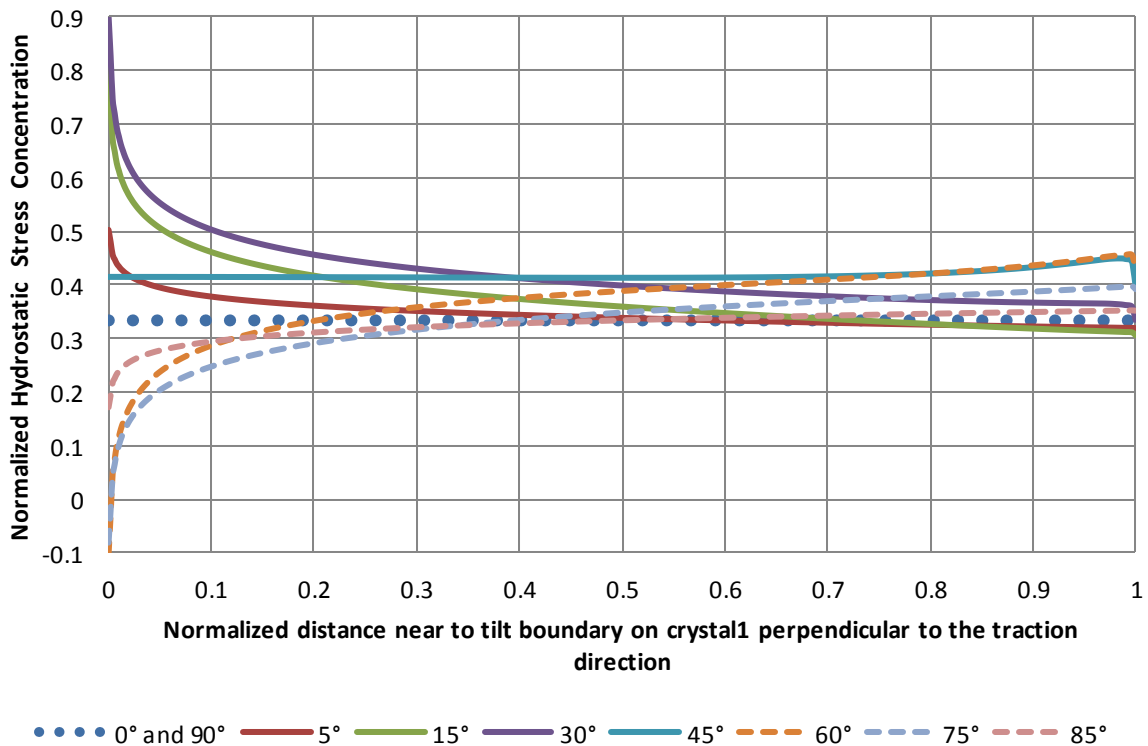

Fig. 3(a) shows the normalized hydrostatic stress concentration (σ_H/σ_0) along the normalized path on the GBAZ on the fixed crystal perpendicular to the traction direction for various misorientation angles.
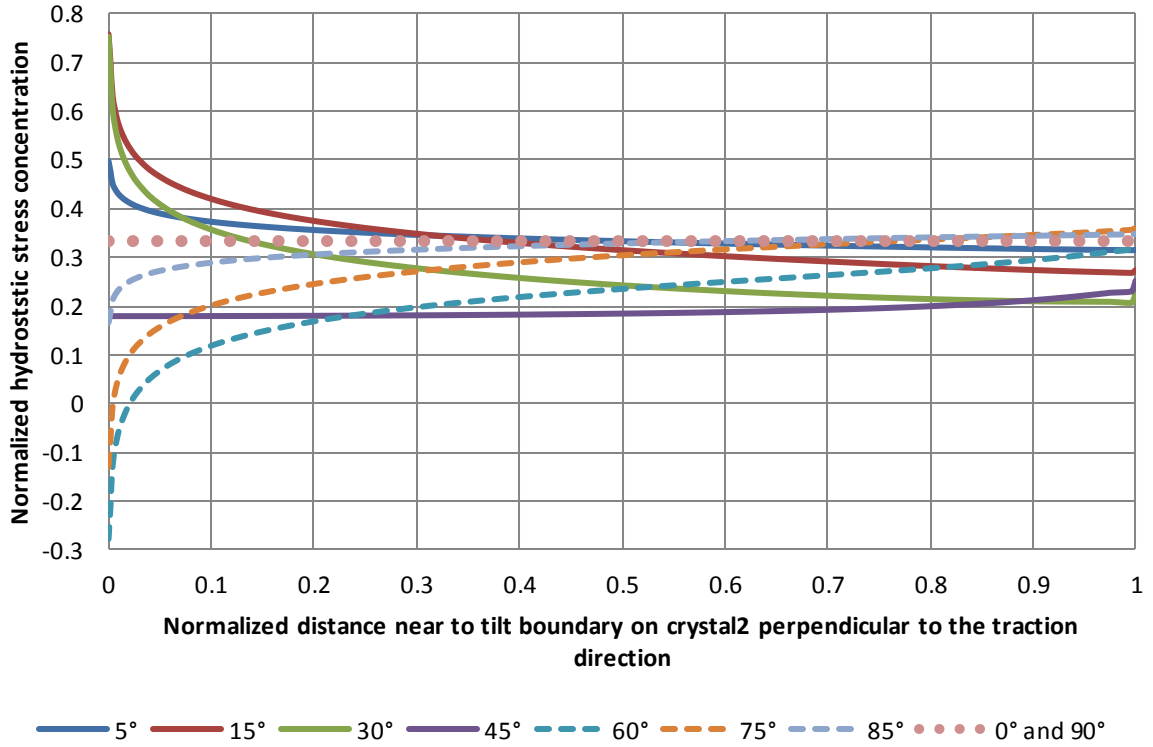
Fig. 3(b) shows the normalized hydrostatic stress concentration (σ_H/σ_0) along the normalized path on GBAZ on crystal2 perpendicular to the traction direction for various misorientation angles.
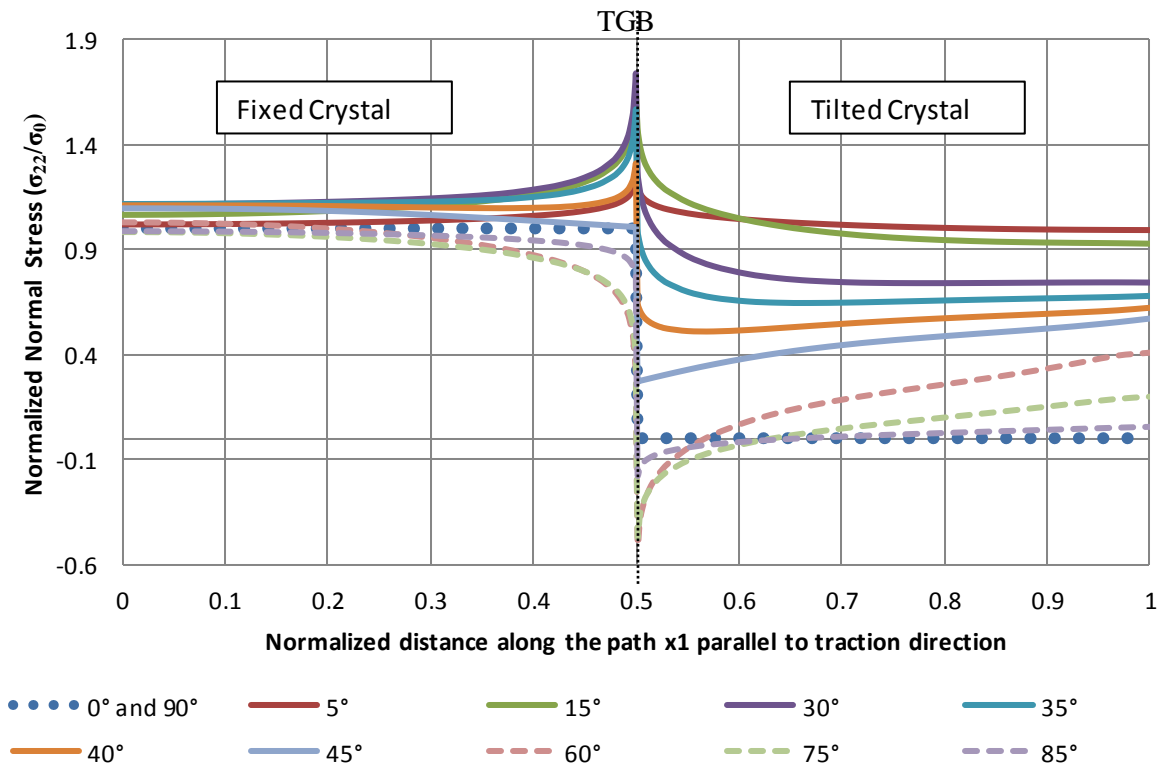
Fig. 4(a) shows the normalized normal stress concentration (σ_{22}/σ_0) along the normalized path x1 parallel to the traction direction for various misorientation angles.
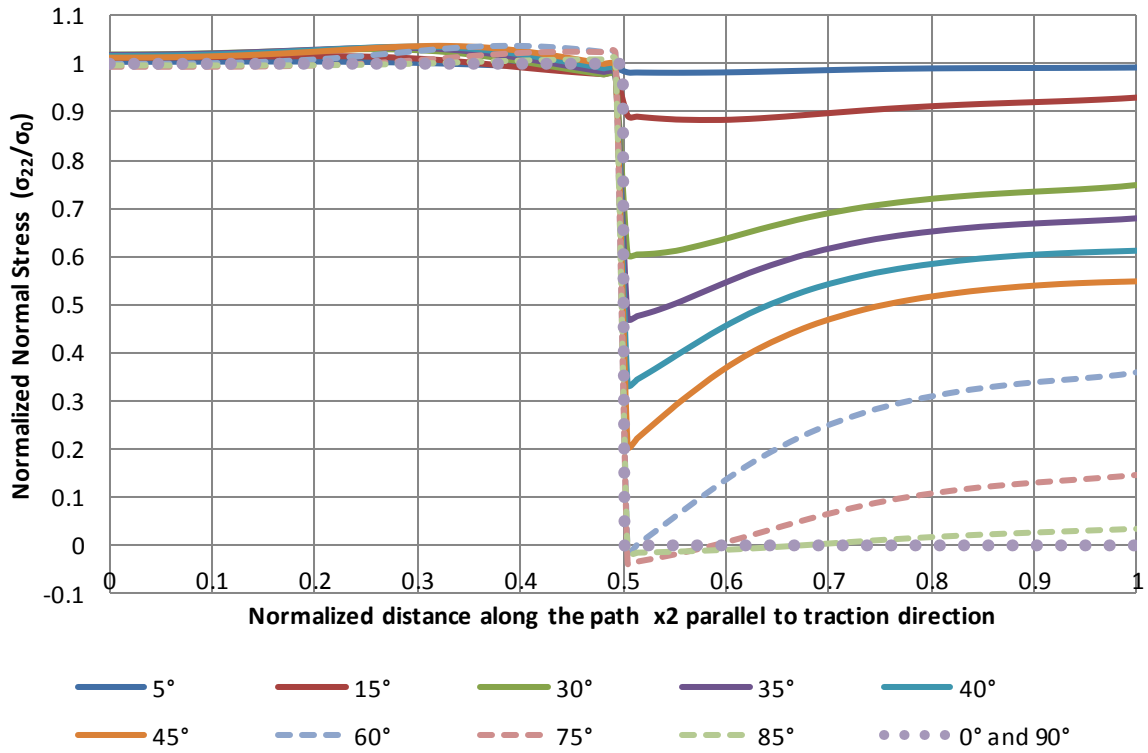
Fig. 4(b) shows the normalized normal stress concentration (σ_{22}/σ_0) along the normalized path x2 parallel to the traction direction for various misorientation angles.
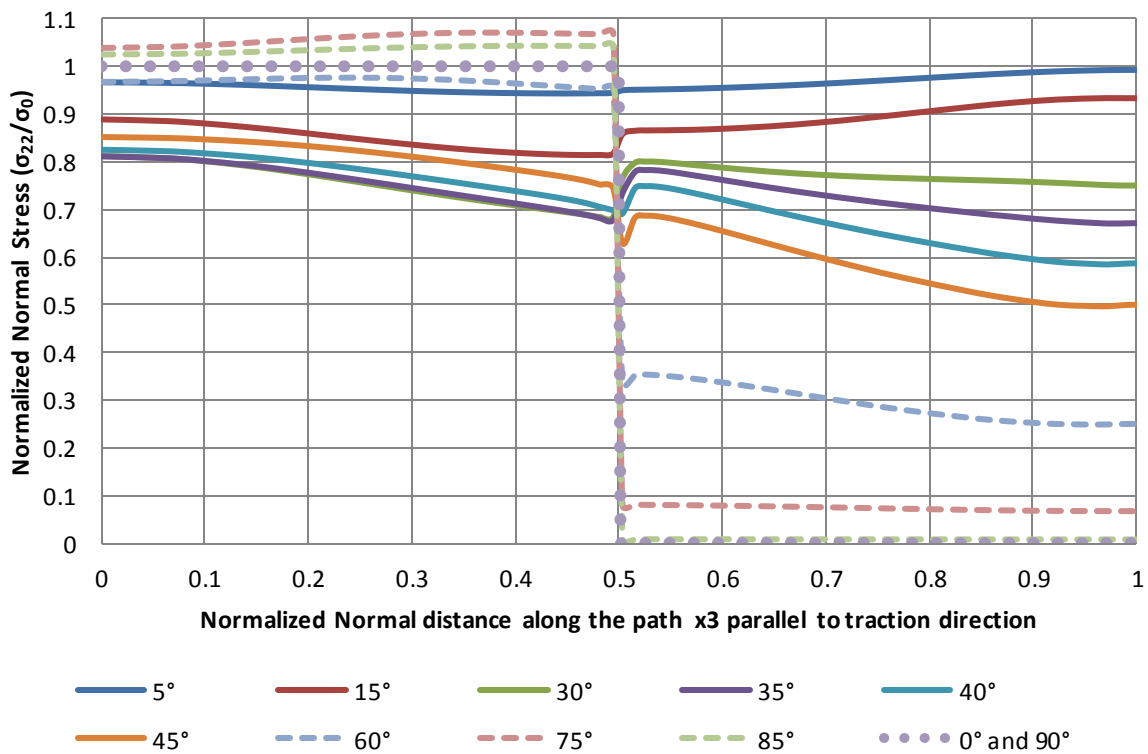
Fig. 4(c) shows the normalized normal stress concentration (σ_{22}/σ_0) along the normalized path x3 parallel to the traction direction for various misorientation angles.
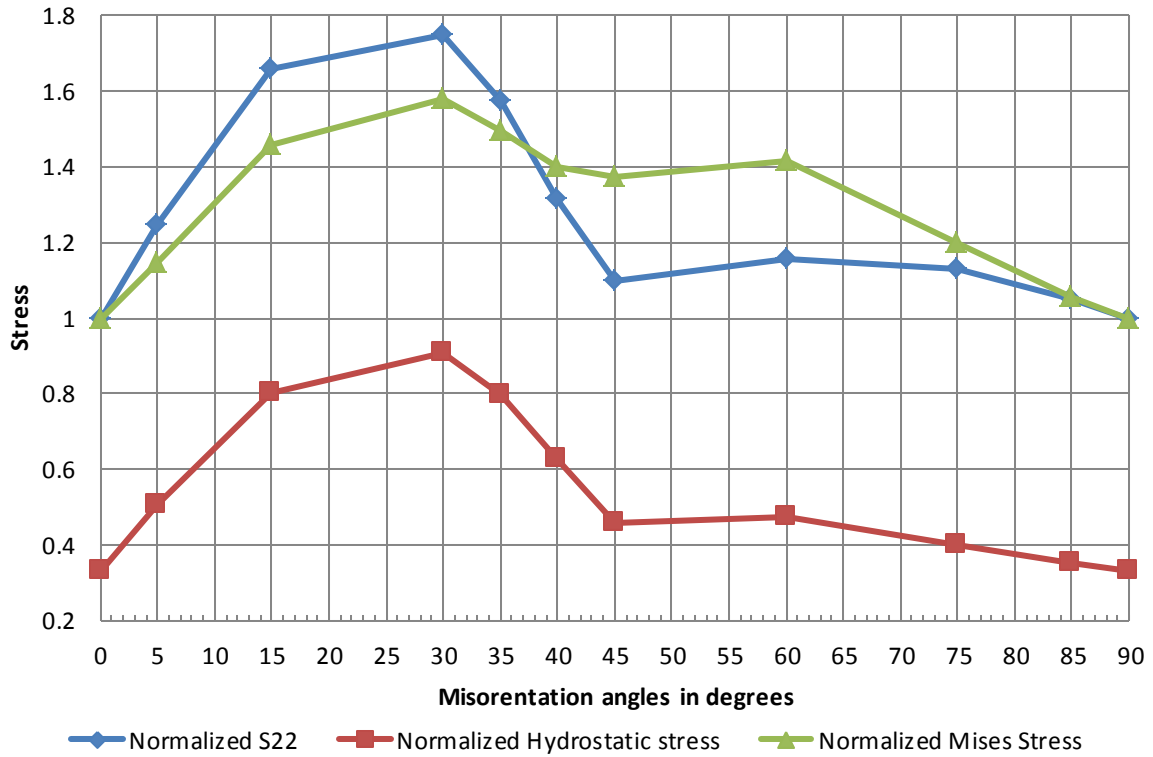
Fig. 5 Shows the maximum normalized normal stress S22 (blue colour), maximum normalized hydrostatic stress (red colour) and maximum normalized Von Mises stress as a function of GB misorientation.
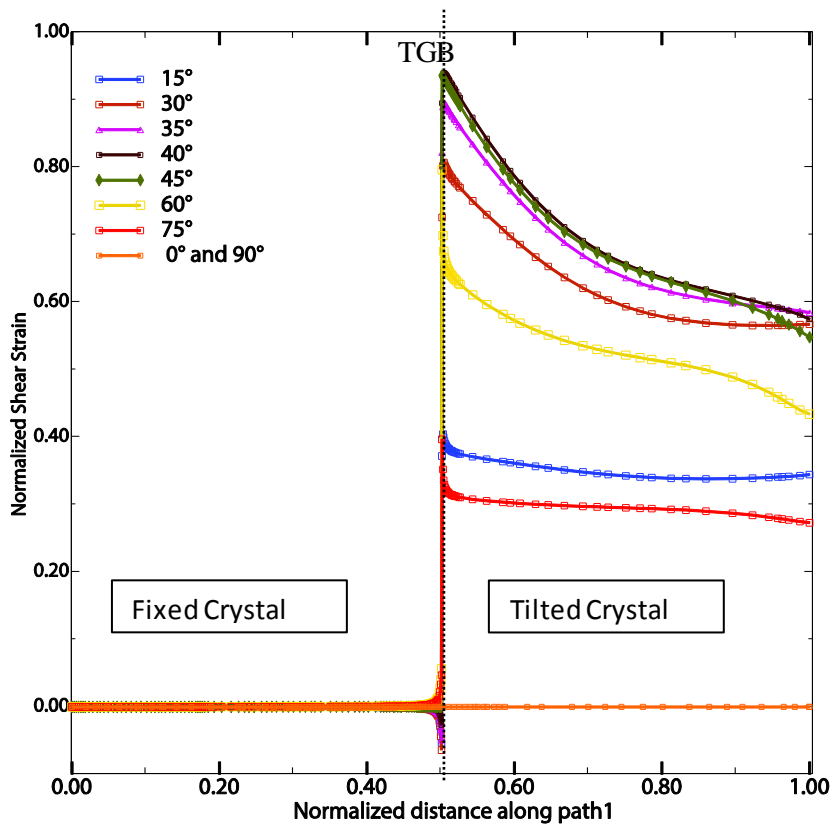
Fig. 6 (a) Shows the normalized shear strain $(\varepsilon_{12}/\varepsilon_0)$ along the normalized path x1 (y/h) parallel to the traction direction [010] for various misorientation angles.
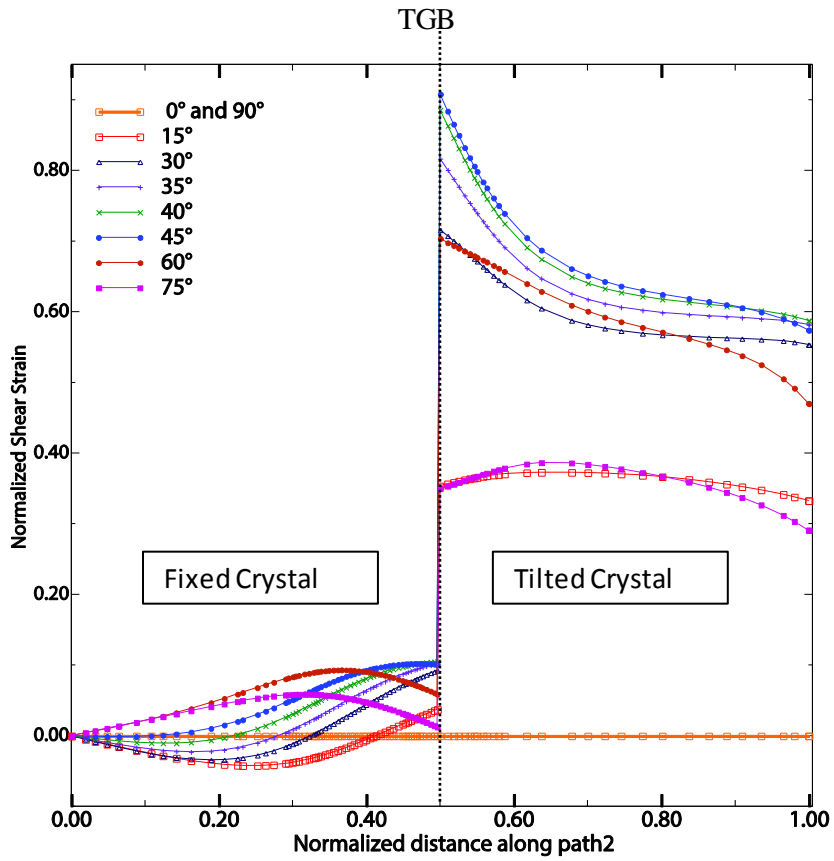
Fig. 6 (b) Shows the normalized shear strain $(\varepsilon_{12}/\varepsilon_0)$ along the normalized path x2 (y/h) parallel to the traction direction for various misorientation angles.
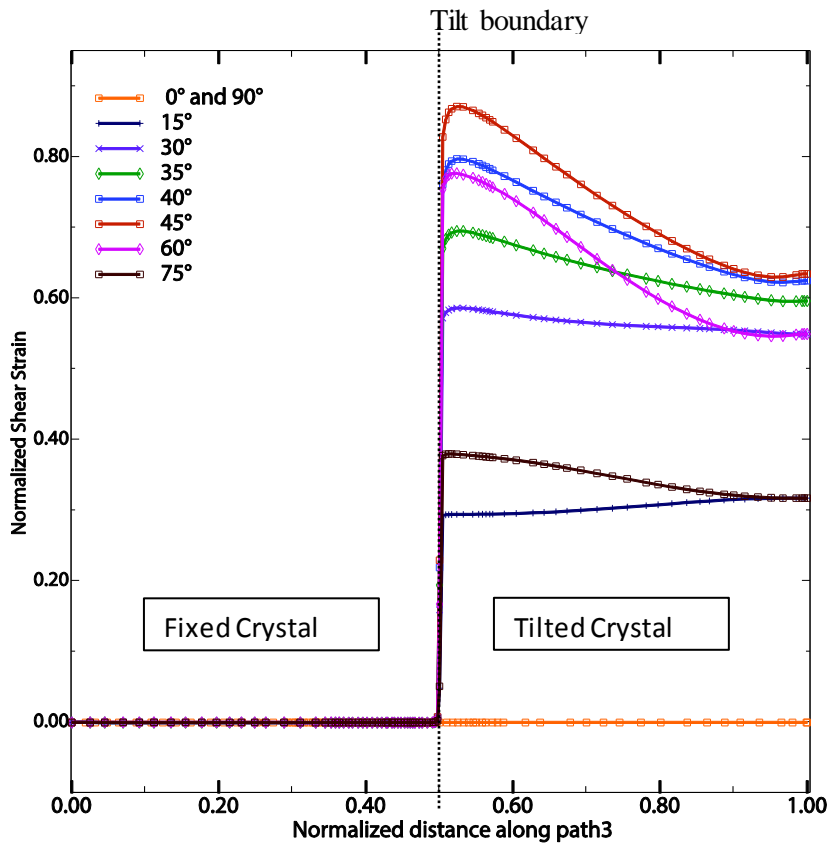
Fig. 6 (c) Shows the normalized shear strain $(\varepsilon_{12}/\varepsilon_0)$ along the normalized path x3 (y/h) parallel to the traction direction for various misorientation angles.
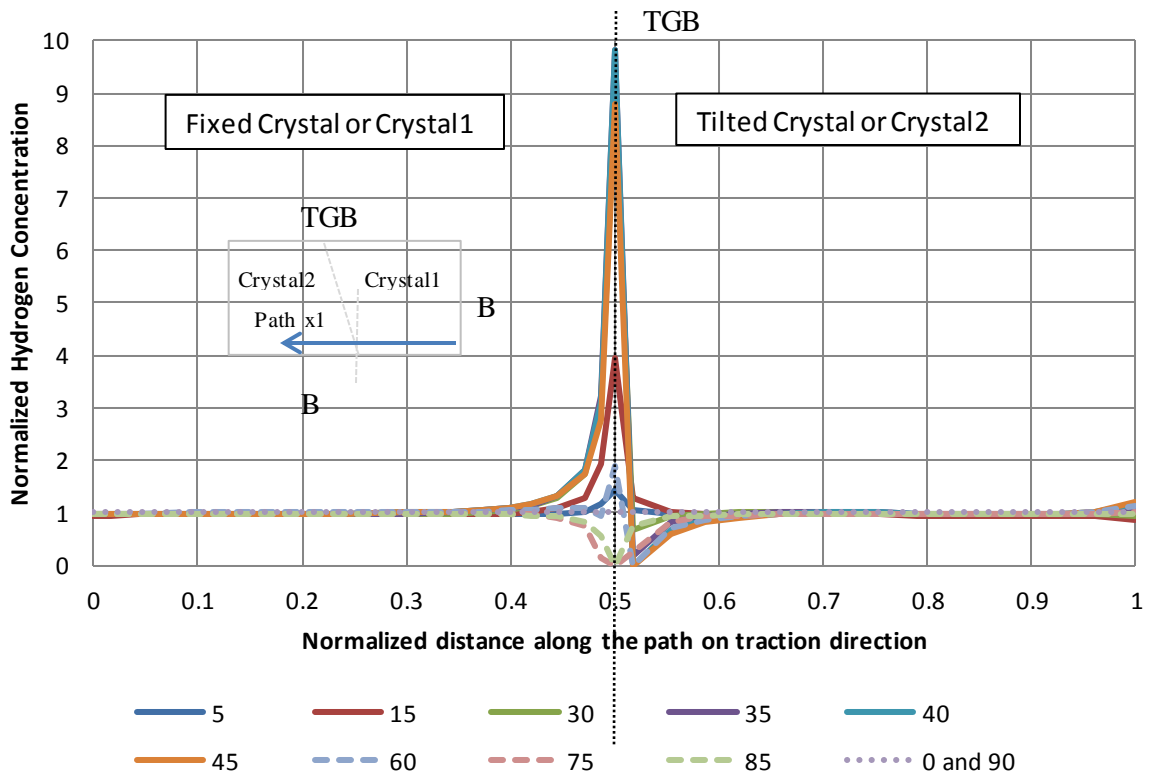
Fig. 7 (a) shows the normalized hydrogen concentration along the normalized path x1 (y/h) parallel to the traction direction for various misorientation angles.
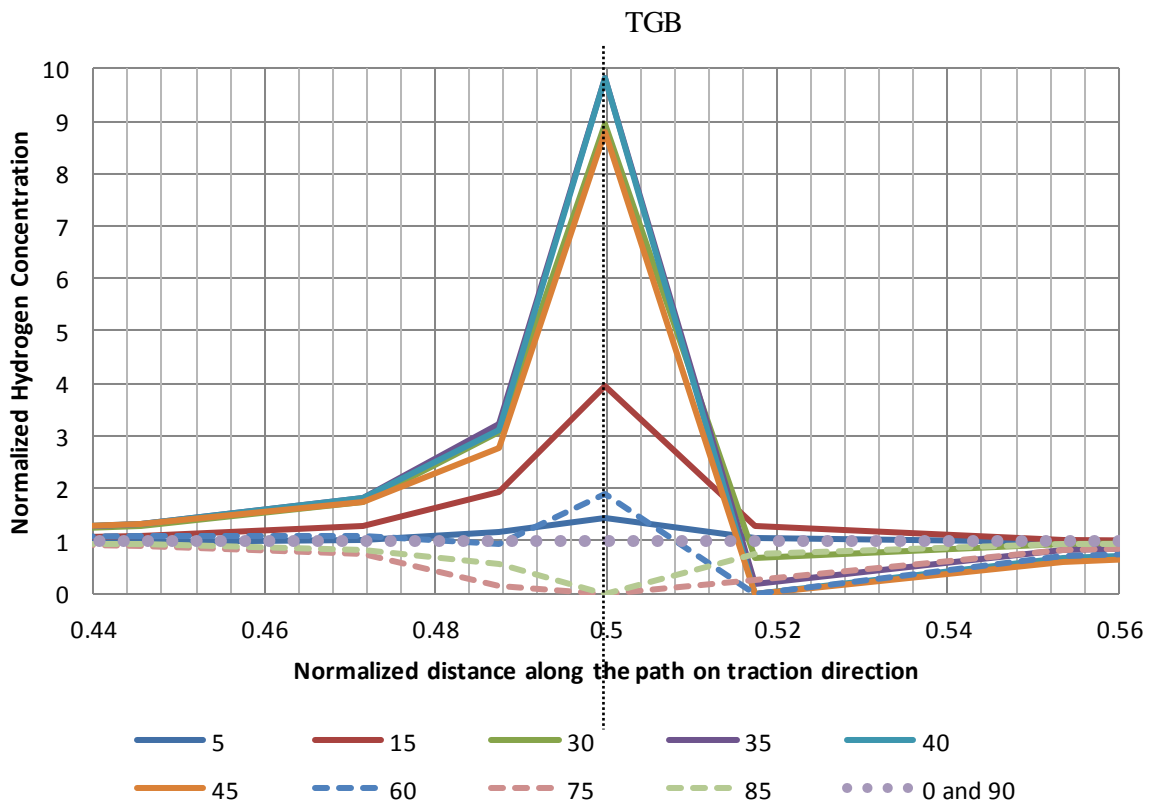
Fig. 7 (b) shows the close view of normalized hydrogen concentration along the normalized path x1 (y/h) parallel to the traction direction for misorientation angles in degrees.
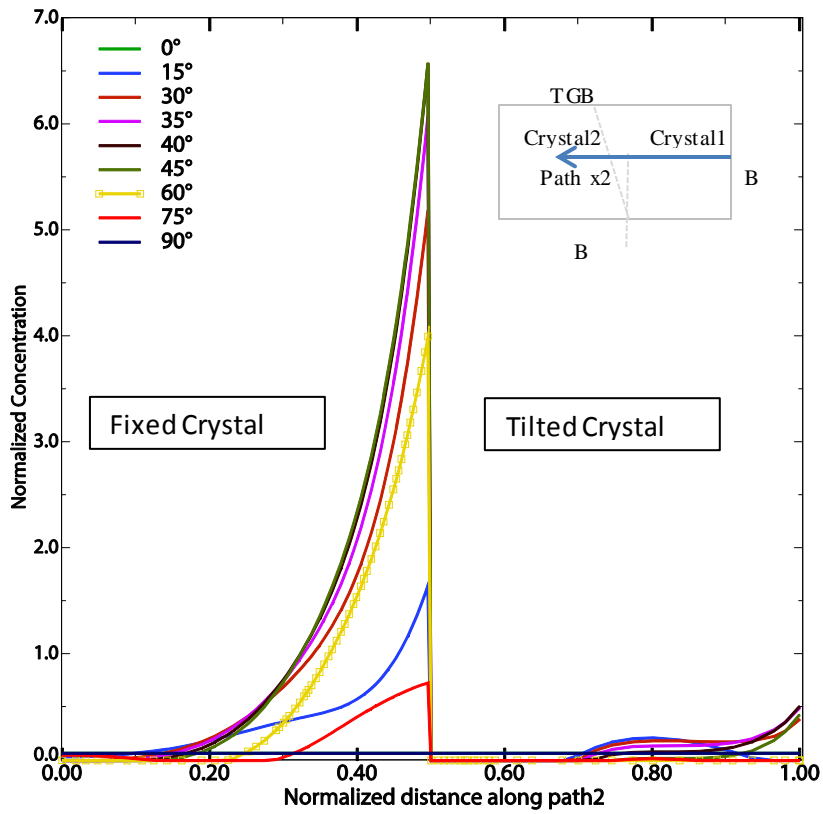
Fig. 8 Shows the normalized hydrogen concentration along the normalized path x2 (y/h) parallel to the traction direction for various misorientation angles after a normalized time=3.
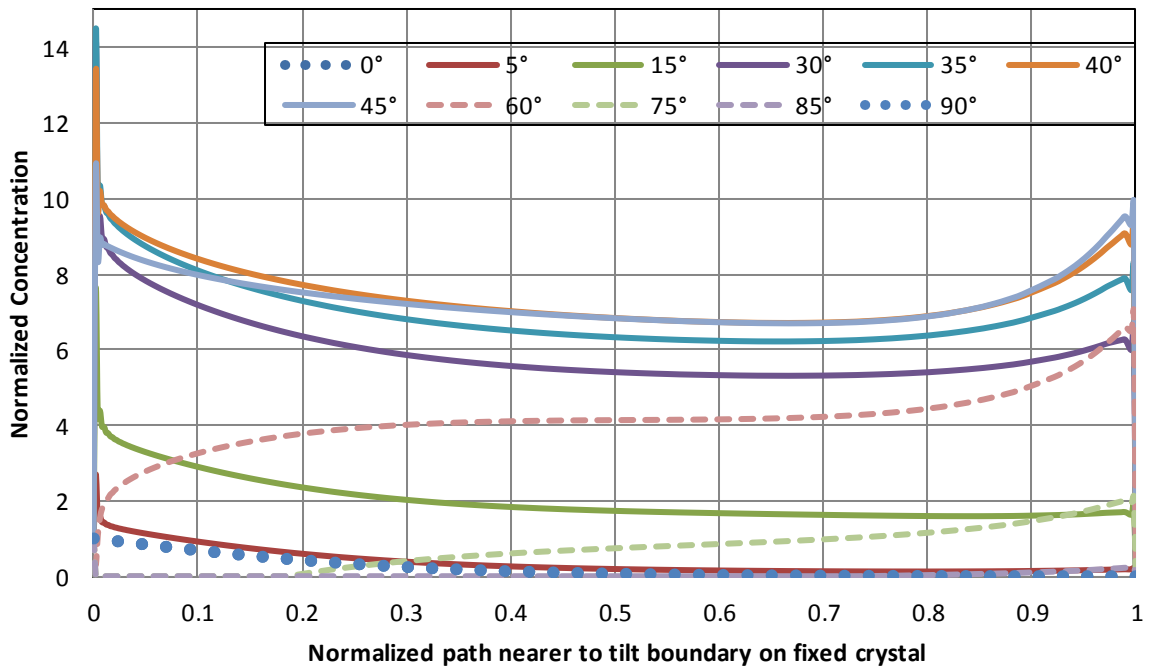
Fig. 9 (a) Shows the normalized hydrogen concentration along the normalized path nearer to TGB on the fixed crystal perpendicular to the traction direction for various misorientation angles.
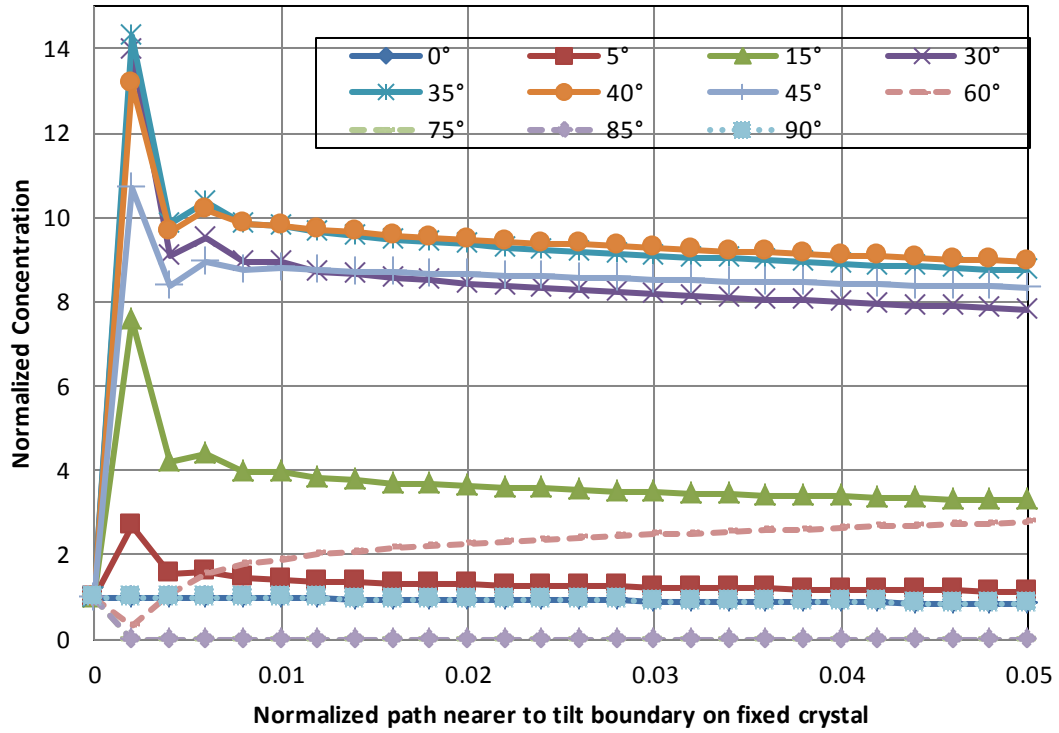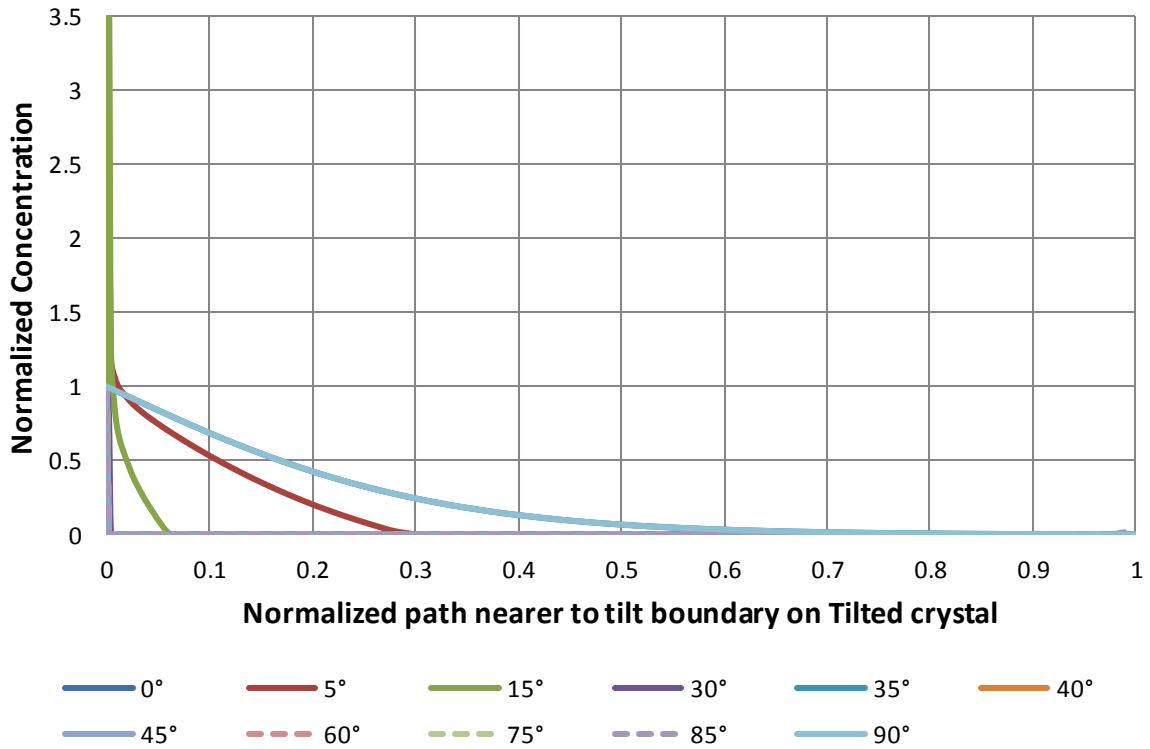
Fig. 9 (b) Shows the close view of normalized hydrogen concentration along the normalized path nearer to TGB on the fixed crystal perpendicular to the traction direction for various misorientation angles.
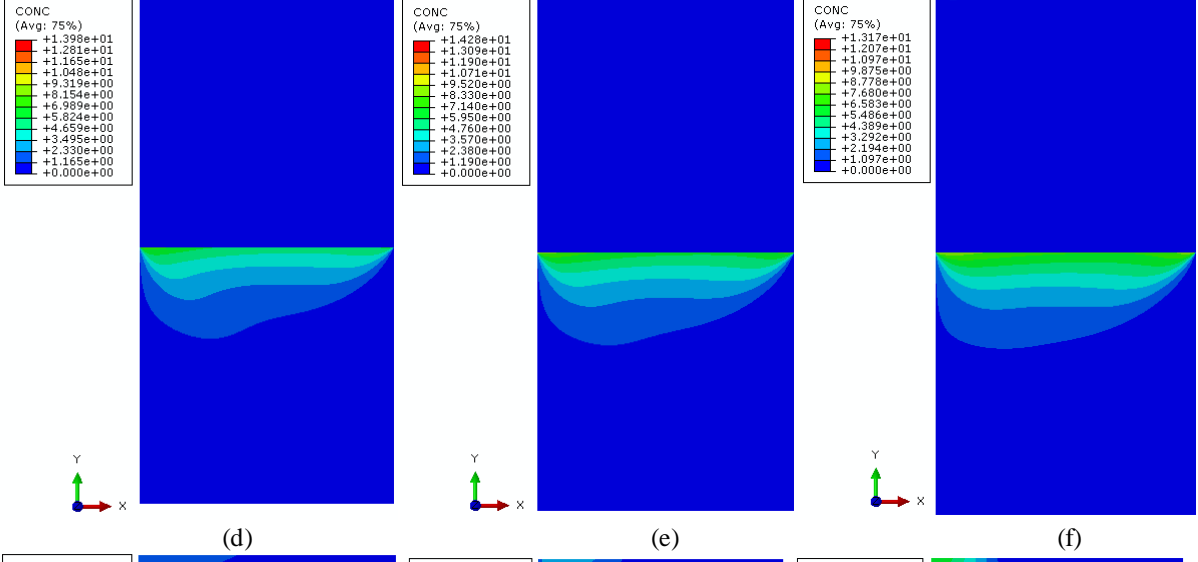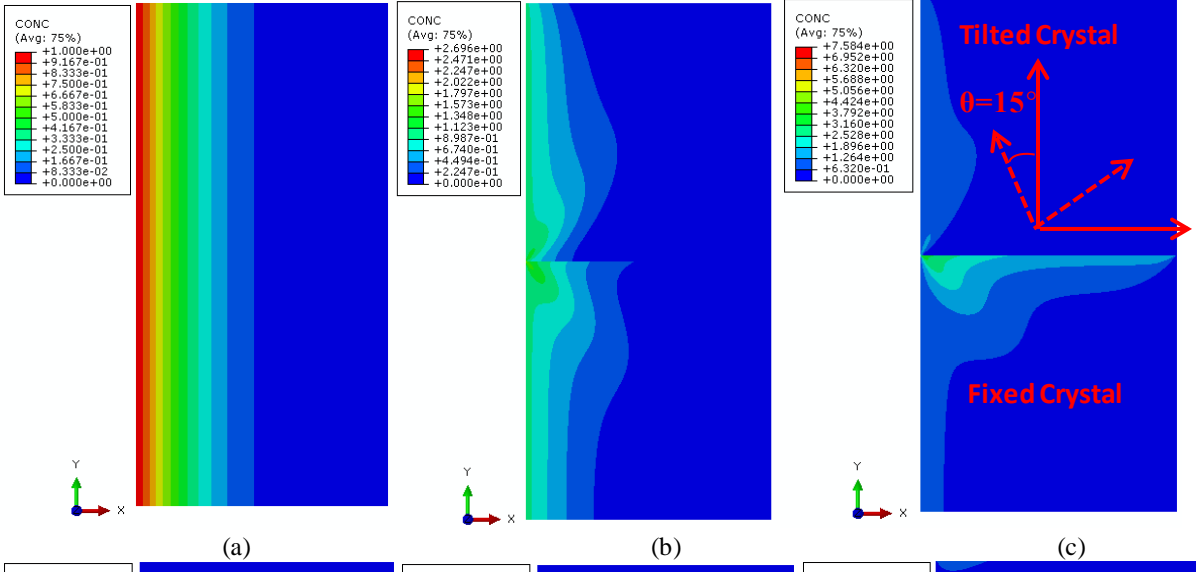

Fig. 10 shows the normalized hydrogen concentration along the normalized path nearer to TGB on crystal2 perpendicular to the traction direction for various misorientation angles.

(a)

(b)

(c)

(d)

(e)

(f)

(g)

(h)

(i)

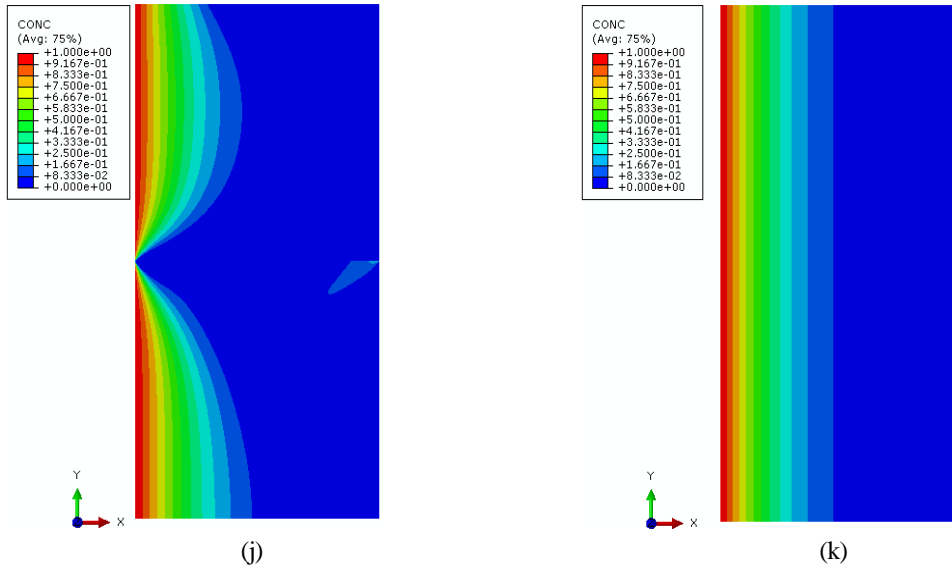(j)   (k)
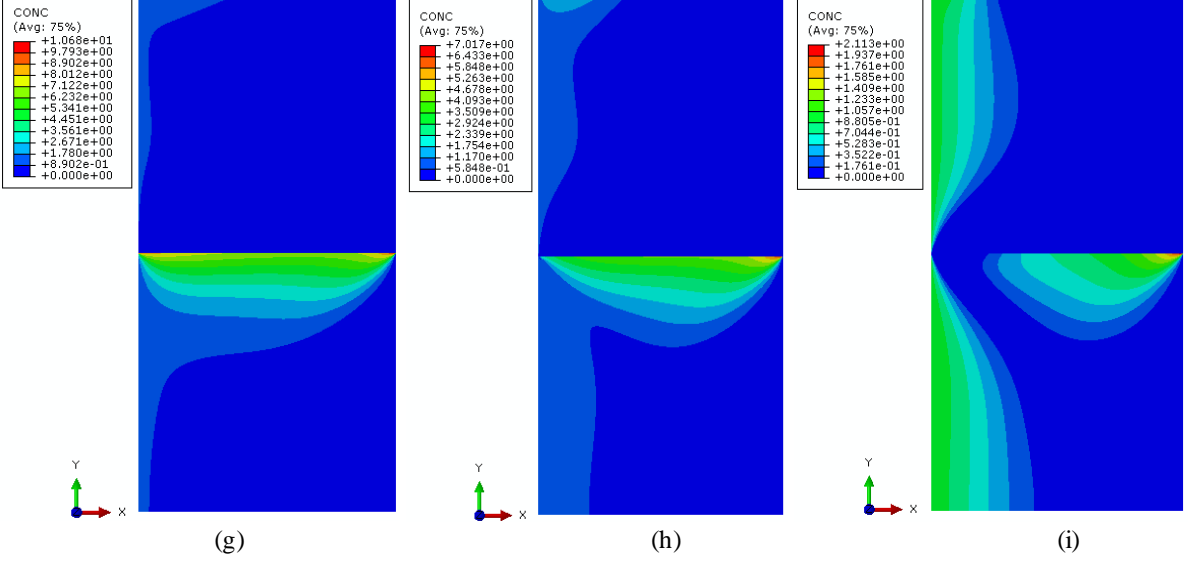
Fig. 11 Shows the counter plot of normalized hydrogen concentration for various misorientation angles in degree after normalized time=3 (a) 0° (b) 5°(c) 15° (d) 30° (e) 35°(f) 40° (g) 45° (h) 60° (i) 75° (j)85° (k) 90°.
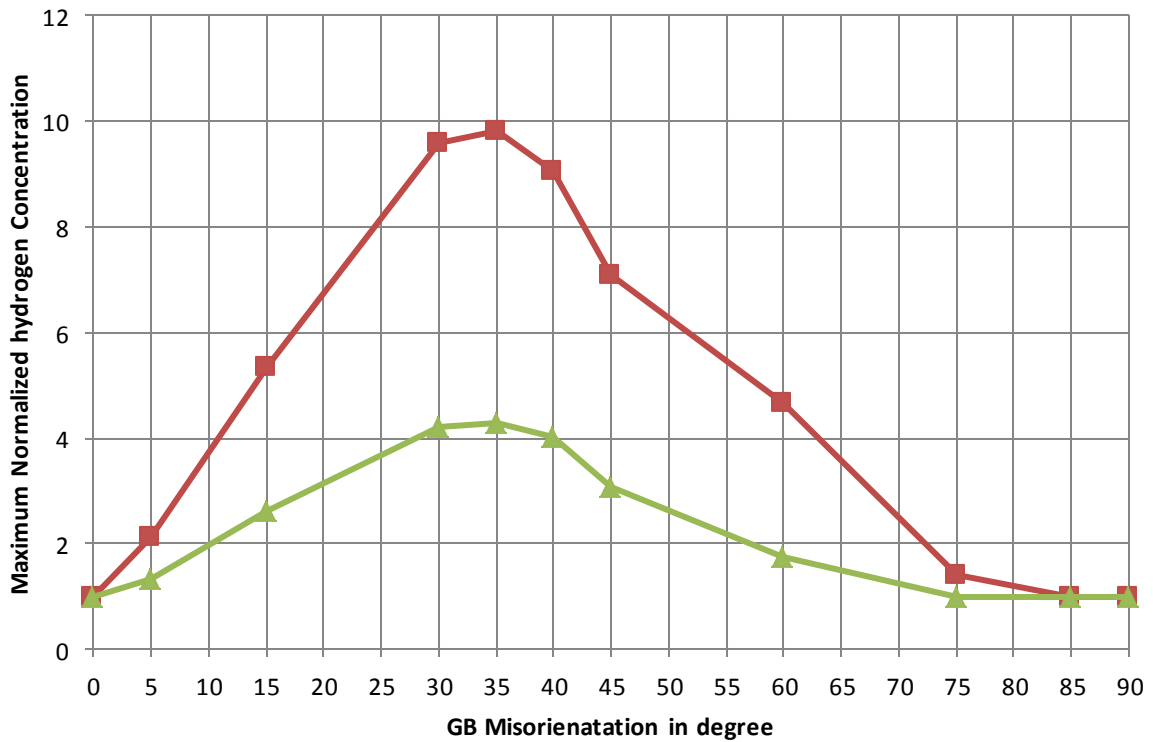

Fig. 12 Shows the maximum normalized hydrogen concentration as the function of misorientation angles in degree after normalized time=1(green colour) and normalized time=2 (red colour).